Ultra-High-Response, Multiply Twisted Electro-optic Chromophores: Influence of π-System Elongation and Interplanar Torsion on Hyperpolarizability

Yanrong Shi,[†,∥] David Frattarelli,[†,∥] Naoki Watanabe,[†] Antonio Facchetti,[†] Elena Cariati,[‡] Stefania Righetto,[‡] Elisa Tordin,[‡] Cristiano Zuccaccia,[§] Alceo Macchioni,[§] Staci L. Wegener,[†] Charlotte L. Stern,[†] Mark A. Ratner,*[,†] and Tobin J. Marks*[,†]

[†]Department of Chemistry and the Materials Research Center, Northwestern University, 2145 Sheridan Road, Evanston, Illinois 60208-3113, United States

[‡]Dipartimento di Chimica dell'Università di Milano and Unità di Ricerca dell'INSTM di Milano, Via Golgi 19, I-20133 Milano, Italy

[§]Dipartimento di Chimica, Biologia e Biotecnologie and CIRCC, Università degli Studi di Perugia, Via Elce di Sotto, I-06123 Perugia, Italy

ⓢ *Supporting Information*

ABSTRACT: The systematic synthesis, structural, optical spectroscopic, and second-order nonlinear optical (NLO) characterization of a series of donor−acceptor poly-arylene chromophores which have heretofore unachieved π-extension and substantial twisting from planarity, are reported: specifically, two-ring **2TTMC**, dicyano(4-(3,5-dimethyl-1-(2-propylheptyl)pyridin-1-ium-4-yl)-3-methylphenyl)methanide; three-ring **3TTMC**, dicyano(4′-(3,5-dimethyl-1-(2-propylheptyl)pyridin-1-ium-4-yl)-2,2′,3′,5′,6′-pentamethyl[1,1′-biphenyl]-4-yl)methanide; and four-ring **4TTMC**, dicyano(4″-(3,5-dimethyl-1-(2-propylheptyl)-pyridin-1-ium-4-yl)-2,2′,3″,6,6′-pentamethyl[1,1′:4′,1″-terphenyl]-4-yl)methanide. Single-crystal X-ray diffraction, DFT-optimized geometries, and B3LYP/INDO-SOS analysis identify three key features underlying the very large NLO response: (1) For ring catenation of three or greater, sterically enforced π-system twists are only essential near the chromophore donor and acceptor sites to ensure large NLO responses. (2) For synthetic efficiency, deletion of one *ortho*-methyl group from *o,o′,o″,o‴*-tetramethylbiaryl junctures, only slightly relaxes the biaryl twist angle from 89.6° to ∼80°. (3) Increased arylene catenation from two to three to four rings (**2TTMC**→ **3TTMC** → **4TTMC**) greatly enhances NLO response, zwitterionic charge localization, and thus the ground-state dipole moment, consistent with the contracted antiparallel solid-state π−π stacking distances of 8.665 → 7.883 → 7.361 Å, respectively. This supports zwitterionic ground states in these chromophores as do significant optical spectroscopic solvatochromic shifts, with aryl−aryl twisting turning on significant intra-subfragment absorption. Computed molecular hyperpolarizabilities ($\mu\beta$) approach an unprecedented 900 000 × 10^{-48} esu, while estimated chromophore figures of merit, $\mu\beta_{vec}/M_w$, approach 1500 × 10^{-48} esu, 1.5 times larger than the highest known values for twisted chromophores and >33 times larger than that of planar donor−acceptor chromophores.
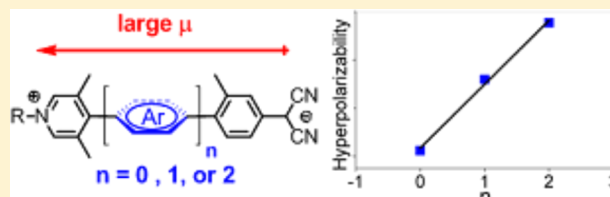
■ INTRODUCTION

The design and realization of large-response organic electro-optic (EO) materials has constituted an active worldwide research area for decades.[1−3] These materials offer the potential of greatly improved means to generate, process, transmit, detect, switch, and store optical signals compared to their inorganic counterparts (e.g., LiNbO₃).[4] Understanding how to enhance molecular EO material properties offers further insight into how soft matter interacts with light, as well as the opportunity to advance technologies such as optical communications, optical data storage, image reconstruction, and optical computing.[1] Given that chromophoric molecular building blocks are the active components of organic EO materials, EO devices with greater bandwidths and lower driving voltages will require larger molecular hyperpolarizabilities (β) than

currently available, as well as high thermal stability and stable bulk non-centrosymmetric alignment.[1−3]

The majority of known EO chromophores with the aforementioned properties have traditionally been designed using similar approaches: planar conjugated π-electron systems end-capped with electron donor (D) and acceptor (A) moieties.[5] This design strategy invariably creates a strong intramolecular optical charge-transfer (ICT) transition from the ground state to the first excited state, while producing strong polarization along the π-conjugation axis. To date, molecular engineering of such structures has adhered to a classical and qualitative "two-level model", which has proven pragmatically

successful in predicting β as a function of chromophore geometry and substitution.[6] In this model, molecular hyperpolarizability, β, is determined by three key factors: (1) the difference in the dipole moments between the ground state and first charge-separated excited electronic state ($\Delta\mu_{ge} = \mu_{ee} - \mu_{gg}$); (2) the transition dipole matrix element connecting these states (μ_{ge}); and (3) the energy gap (ΔE_{ge}) between these states (eq 1). Taking each of these variables into consideration,

$$\beta \propto \Delta\mu_{ge}(\mu_{ge})^2/(\Delta E_{ge})^2 \tag{1}$$

β should be tunable via appropriate structural modifications. To date, several design strategies have proven effective in enhancing molecular hyperpolarizability. One approach by Marder and co-workers involves tuning "bond length alternation" (BLA), the difference between the average single and double bond lengths in the conjugated chromophore core.[7] It is argued that β can be optimized by controlling the relative neutral and charge-separated contributions to the electronic ground state by modifying the (1) D/A substituent strength, (2) polarity of the solvent, and/or (3) strength of the applied field. Another "auxiliary donors and acceptors" model correlates molecular hyperpolarizability with the electron density of the π-conjugation, crediting substantial increases in β values to electron-excessive/deficient heteroaromatic bridges.[8] Here, hyperpolarizability enhancements are largely attributed to compressing the energy gap (ΔE_{ge}) in eq 1 (e.g., CLD, Chart 1).[2o] Nevertheless, it is known that large-response chromophores, based only on extensive planar π-conjugation, tend to be complex, synthetically challenging, and frequently exhibit chemical, thermal, and photochemical instabilities.[9] Furthermore, extended conjugated systems typically introduce bathochromic shifts in the optical absorption, eroding near-IR

transparency at the working wavelengths of most photonic technologies. Other recently developed β enhancement strategies to improve near-IR transparency include multidimensional charge-transfer (CT) chromophores (e.g., HPEB and X-CHR, Chart 1)[10] and planar zwitterionic chromophores (e.g., PCTCN, Chart 1).[2d,11]

Another chromophore design strategy receiving significant attention, both theoretically and experimentally, is the twisted molecular charge-transfer (TICT) approach (e.g., TMC-3, Chart 1; TICTOID chromophores, Chart 2).[12] Here, TICT β response correlates with twisting from planarity about the bond linking the conjugated D–A π-arene systems, thereby reducing orbital overlap between these fragments. This approach offers a mechanism by which nearly complete charge transfer can occur upon optical excitation, greatly enhancing CT interactions and affording unprecedented hyperpolarizabilities.[12b,13] Recent theoretical and experimental studies established the importance of sterically induced dihedral twisting in amplifying the hyperpolarizability of zwitterionic chromophores bearing various D/A substituent combinations, sterically encumbered twist-enhancing substituents, conjugation length, and bulky dendritic additions to minimize aggregation.[2a,14] It was shown that such chromophores can have relatively simple, robust biaryl structures with twist angles tunable via R^1, R^2, R^3, and R^4 modification (Chart 2), from 9° to ~90°, depending on the nature and number of ortho substituents. Both computation and X-ray diffraction confirm these structure–response trends, leading to remarkable $\mu\beta_{vec}$ values as high as $-488\,000 \times 10^{-48}$ esu, measured by electric-field-induced second harmonic generation (EFISH)—the highest chromophore response reported to date (TMC-3, Chart 2).[2a,13,14] In terms of figure of merit, $\mu\beta/M_w$ (M_w = molecular weight), is as large as 9800×10^{-48} esu, almost 20 times larger than the highest molecular

Chart 1. Large-Response Electro-optic Chromophores Previously Reported in the Literature
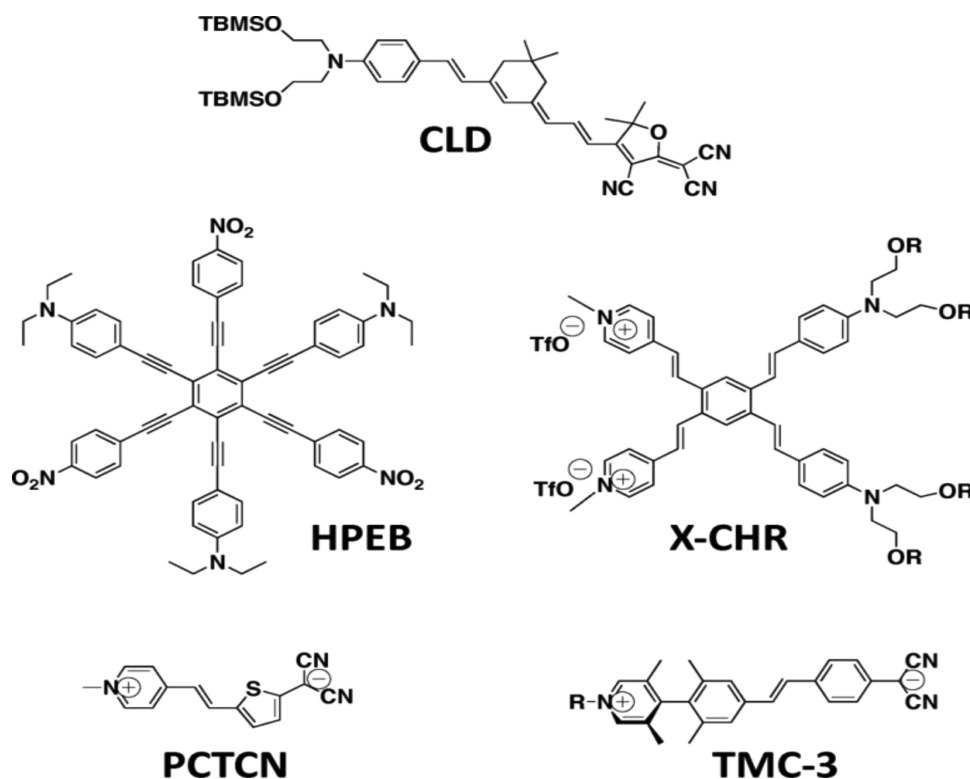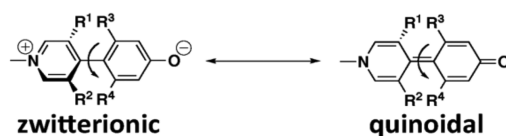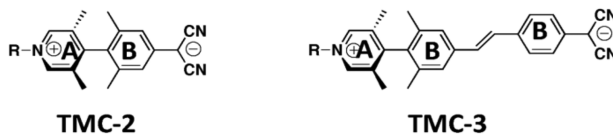
Chart 2. Ultra-Large-Response, Twisted π-System Electro-optic Chromophores
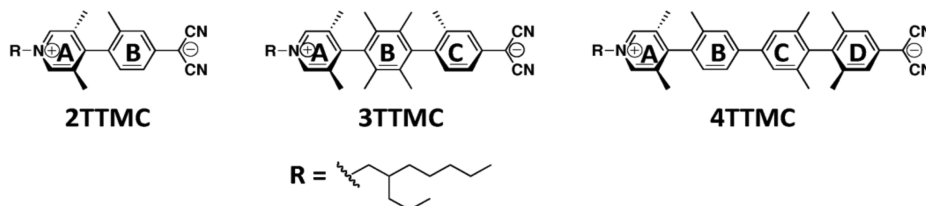

values previously reported. The β enhancement is argued to result from aromatic stabilization and formal charge-separated ground states (modified by polar solvation), leading to large changes in dipole moment ($\Delta\mu_{ge}$), large transition dipole matrix elements (μ_{ge}), and relatively low-energy optical excitations (ΔE_{ge}). From the two-level model of eq 1, note that these factors should all enhance β.[2a] Beyond twist angle-sensitivity, TICT molecules also exhibit large β sensitivities to environmental polarity (e.g., neighboring crystal lattice molecules, solvation, and/or applied fields).[2a,14b,c] For all of these reasons, zwitterionic TICT molecules have proven both scientifically and technologically intriguing.

To date, all TICT chromophore studies have focused on twist angle manipulation, with minimal consideration of charge separation effects.[2a,13,14] Traditionally, planar chromophore π-backbones were designed to optimize ICT via extended conjugation and/or enhanced polarization (e.g., **CLD**; Chart 1). This includes introducing heterocycles having aromatic stabilization and extended planarity, but without resonance destabilizing effects.[15] One chromophore series that minimized aromatic destabilization energy costs, without using hetero-aromatic rings, are twisted **TMC** chromophores (Charts 1 and 2).[2a,13,14] Nevertheless, despite the exceptional β responses, "champion" **TMC-3** contains a stilbene fragment which is not optimal for photo-oxidative stability.[16] While arene fragments can resist these effects, aromatic stabilization may depress transition moments and increase ground-state to first excited-state excitation energies, reducing β in the two-level model.[15] To address reduced aromatic stabilization, the two most successful approaches to date are (1) replace aromatic groups with heterocycles[15] and (2) introduce twisted biaryl fragments.[2a] The latter approach has the advantage of increasing D/A zwitterionic charge separation as discussed above. In chromophore **TMC-3**, the replacement of the styryl unit with a twisted biaryl subunit should reduce aromatic delocalization while enhancing charge localization. This would enhance the transition moment and dipole moment change, while

decreasing the excitation energy in eq 1, thereby greatly enhancing β.

To systematically probe TICT architecture−electronic structure−hyperpolarizability correlations, we report here the new chromophore series, **2TTMC**, **3TTMC**, and **4TTMC** (Chart 2), that is structurally similar to **TMC-2**, but with increased D/A charge separation via progressive phenylene catenation: **2TTMC → 3TTMC → 4TTMC**. The effects of the number and location of methyl substituents to enforce conformational twists within the biaryl junctions are assessed across the series. The derivatives of **2TTMC** with variations of N-alkyl substituents (−R) on pyridinium moiety (**2TTMC-a** and **2TTMC-b**) are also introduced to compare aggregation effects. We discuss in full detail new synthetic approaches, solution and solid-state structures, electronic structures, aggregation characteristics in solution, and NLO/EO response properties using an array of techniques, including X-ray diffraction, cyclic voltammetry, solvent- and concentration-dependent linear optical spectroscopy, diffusion NMR spectroscopy, and solution-phase DC EFISH spectroscopy, combined with B3LYP/INDO-SOS computational analysis. It will be seen that molecular hyperpolarizabilities ($\mu\beta$) approach an unprecedented $900\,000 \times 10^{-48}$ esu, while chromophore figures of merit, $\mu\beta_{vec}/M_w$, approach 1500×10^{-48} esu, 1.5 times larger than previous values for twisted chromophores and >33 times larger than that of planar D−A chromophores.

■ EXPERIMENTAL SECTION

Materials and Methods. All reagents were purchased from Sigma-Aldrich Co. and used as received unless otherwise indicated. Tetrahydrofuran (THF) was distilled from Na/benzophenone, and CH_2Cl_2 from $CaCl_2$. $CHCl_3$ was dried and distilled from anhydrous K_2CO_3. Toluene and pentane were each dried by passing through packed columns of activated alumina and Q5 under N_2, following testing with benzophenone ketyl in ether solution. The reagent 2-propyl-1-heptanol was purchased from Narchem Co. The reagents 4-bromo-3,5-dimethylpyridine 1-oxide (**1**),[17] 4,4′-dibromo-2,2′,6,6′-tetramethyl-1,1′-biphenyl (**20**),[18] and the ligand dicyclohexyl(2-phenanthren-9-yl-phenyl)phosphane (**DCPPP**), for catalytic Suzuki

Scheme 1. Synthesis of Twisted Chromophore 3TTMC[a]
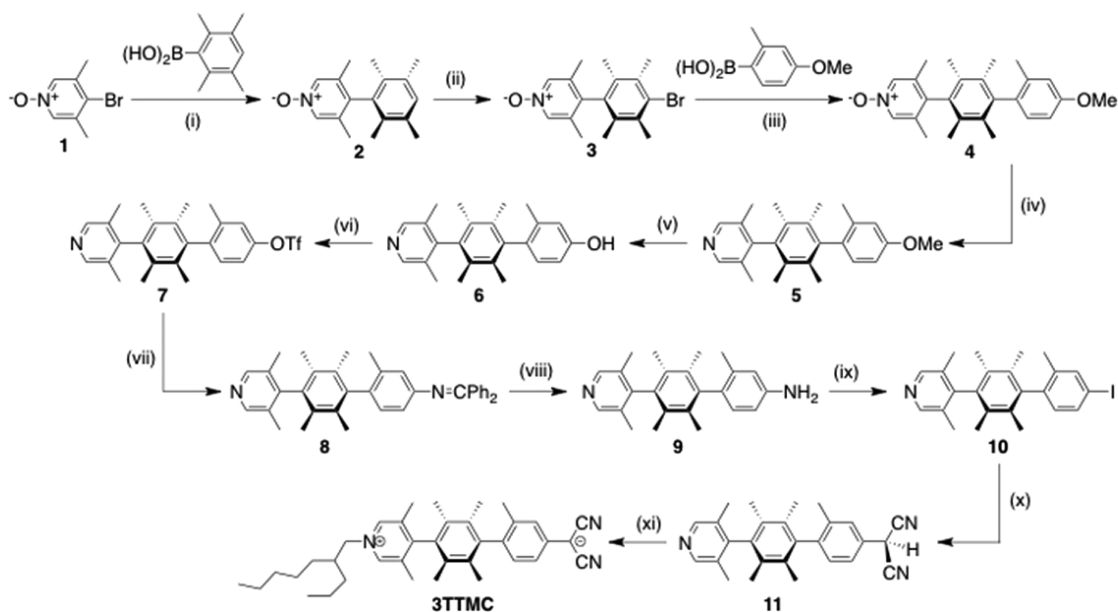
[a]Reagents and conditions: (i) Pd$_2$(dba)$_3$/DCPPP, Ba(OH)$_2$, toluene; (ii) FeCl$_3$, Br$_2$, CHCl$_3$; (iii) Pd$_2$(dba)$_3$/Sphos, Ba(OH)$_2$, toluene; (iv) NaH$_2$PO$_2$, Pd/C, AcOH; (v) pyridineH$^+$Cl$^-$; (vi) Tf$_2$O, pyridine; (vii) NH=CPh$_2$, Pd(OAc)$_2$/BINAP, Cs$_2$CO$_3$, THF; (viii) NH$_2$OHHCl, NaOAc, MeOH; (ix) NO$^+$BF$_4^-$, CH$_3$CN, NaI; (x) NaCH(CN)$_2$, Pd(PPh$_3$)$_4$, DME; (xi) C$_{10}$H$_{21}$OTf, CH$_2$Cl$_2$, MeONa, MeOH.

coupling, were synthesized according to literature procedures (Scheme 1).[19a] NMR spectra were recorded on Varian Mercury-400 MHz or INOVA-500 MHz spectrometers. Mass spectra were recorded on a Micromass Quattro II Triple Quadrupole HPLC/MS/MS mass spectrometer. Elemental analyses were performed by Midwest Microlab. Optical spectra were recorded on a Cary 5000 spectrophotometer under N$_2$. Cyclic voltammetry was performed with a BAS 100 electrochemical analyzer, using a three-electrode cell (carbon working electrode, Ag wire pseudo-reference electrode, Pt wire counter electrode) with 0.1 M Bu$_4$NPF$_6$ in anhydrous MeCN as the electrolyte. All electrochemical potentials are quoted versus the ferrocene/ferrocenium (Fc/Fc$^+$) couple internal standard. Moisture sensitivity studies were performed in NMR tubes using dry 0.5 mM DMSO-d_6 solutions. NMR samples were initially made under N$_2$, and later exposed to moisture in air and measured after: 6 h, 1 day, and 5 days. A drop of 2% HCl solution was then added to complete the reaction. All measurements were performed in the dark.

Single-Crystal X-ray Diffraction. Single crystals of the **TTMC** chromophores were obtained via slow vapor diffusion under N$_2$. A small vial containing a solution of a few mg of each chromophore in 1.0 mL CH$_2$Cl$_2$ and a few drops of MeOH was placed in a closed chamber, into which diethyl ether was added. The small vial was sealed with a plastic cap having a small hole to allow slow diffusion of ether vapor from the chamber into the vial for single crystal growth. All diffraction measurements were carried out on a Bruker SMART CCD diffractometer with graphite-monochromated Mo Kα (0.71073 Å) radiation. Data were collected using the Bruker SMART detector, processed using the Bruker SAINT-NT package, and corrected for Lorentz and polarization effects. The structures were solved by direct methods (SHELXTL-90) and expanded using Fourier techniques (SHELXTL-97). The non-H atoms were refined anisotropically. H atoms on dichloromethane molecules of solvation were refined with group isotropic displacement parameters. The remaining H atoms were included in idealized positions but not refined. All calculations were performed using the Bruker SHELXTL9 crystallographic software packages.

Diffusion NMR Spectroscopy. ^{1}H PGSE diffusion NMR measurements were performed at 295.7 K without spinning using the standard stimulated echo pulse sequence[20] on a Bruker AVANCE DRX 400 spectrometer equipped with a GREAT 1/10 gradient unit

and a QNP probe with a Z-gradient coil. Data acquisition and elaboration were carried out as previously described,[14c] using an HDO sample (0.04%) in D$_2$O for gradient calibration[21] and the residual solvent signals as internal standards to account for possible changes in solution viscosity,[22] temperature and gradient strength reproducibility.[23] The translational self-diffusion coefficient (D_t) experimental error is estimated to be around 5%.

Electric-Field-Induced Second-Harmonic Generation Measurements. Measurements of $\mu\beta_{vec}$, the product of the chromophore dipole moment (μ) and the vector part of the molecular first-order hyperpolarizability β_{vec} tensor along the μ direction, were performed by the solution-phase DC EFISH method,[24] which provides direct information on the intrinsic molecular nonlinear optical (NLO) response via eq 2. Here, $\mu\beta/5kT$ is the dipolar orientational

$$\gamma_{EFISH} = (\mu\beta/5kT) + \gamma(-2\omega; \omega, \omega, 0) \qquad (2)$$

contribution, and $\gamma(-2\omega;\omega,\omega,0)$, the third-order term at frequency ω of the incident light, is the electronic contribution to γ_{EFISH}, which is negligible for molecules of the type investigated here.[25] EFISH measurements were carried out in CH$_2$Cl$_2$ and dimethylformamide (DMF) solutions of different concentrations at a nonresonant fundamental wavelength of 1907 nm using a Q-switched, mode-locked Nd^{3+}:YAG laser [pulse durations of 15 ns (90 ns) at a 10 Hz repetition rate]. The 1064 nm initial wavelength was shifted to 1907 nm by a Raman shifter with a high-pressure H$_2$ cell. The $\mu\beta_{vec}$ values reported (see Table 5) are the averages of 16 successive measurements performed on each sample.

Computation. Using the Maestro interface, **2TTMC**, **3TTMC**, and **4TTMC** (Chart 2) were constructed with initial chromophore geometries computed using finite field methods implemented in Jaguar v5.00.22,[26] with the Maestro Molecular Modeling Interface c5.10. Electronic structure calculations were performed at the B3LYP level.[26,27] Because of the complexity of the large systems in this study and the impact of basis set on optical properties,[28] both diffuse and polarization functions were included via the Pople 3-21+G(d,p) basis set. All geometries were optimized with the ring−ring dihedral angles set initially to 85°. This angle was selected due to its similarity to the dihedral angles of previous TICT systems characterized by X-ray diffraction.[2a,13,14] Thereafter, twist angles were not constrained

during geometry optimizations. All optimizations were performed without symmetry constraints. B3LYP calculations converged to an rms error in the density matrix of at most 10^{-7} and energy of at most 10^{-5} hartrees with **4TTMC**, only converging to 10^{-5} and 10^{-4} hartrees, respectively. Chromophore electronic properties (static dipole moments, transition dipole moments, transition energies) were next evaluated using the computationally efficient semiempirical INDO/S[29] Hamiltonian developed by Zerner and co-workers using the CNDO[30] program. The INDO/S[29] calculation was coupled to a single-configuration interaction (SCI) scheme, which generally provides a reliable description of the properties of one-photon allowed excited states, which are those involved in the perturbative description of the first-order hyperpolarizability.[6a,31] The 70 highest occupied and 70 lowest unoccupied MOs were active in the SCI procedure. Results frequently converged at the 50 × 50 level, which was routinely tested against larger calculations.

Molecular polarizabilities and hyperpolarizabilities (β) were calculated with the sum-over-states (SOS)[32] formalism, using standard perturbation equations with excitation energies, transition dipole moments, and excited-state dipole moments obtained from the INDO/SCI calculations. The first hyperpolarizability β appears as the third-rank tensor in the first nonlinear term that arises, dependent on the induced molecular dipole moment (μ) on the applied electric field (F) experienced by the molecule (eq 3). Here, $\mu_i^{(0)}$ is the

$$\mu_i = \mu_i^{(0)} + \sum_j \alpha_{ij}F_j + (1/2)\sum_{j,k}\beta_{ijk}F_jF_k \qquad (3)$$

permanent dipole moment of the molecule in direction i, F_j is the component of the electromagnetic field in direction j, and α and β are the static (zero frequency, $\omega = 0.0$ eV) first- and second- order polarizability tensors. To avoid issues of resonance enhancement, only

the limiting zero frequency or "static" case ($\omega = 0.0$ eV) is reported here. The β_μ (β_{vector}) component of the β tensor is of interest here. As discussed elsewhere,[14b] simple but pragmatic INDO/S SOS parametrization is not completely accurate for computing the exact response of TICT chromophores, but it is used here to explore and interpret trends in the nonlinear response.

■ RESULTS

We first report the synthesis and characterization of Generation 2 multi-ring TICT chromophores (Chart 2). As in first-generation TICT chromophores previously synthesized in this laboratory,[2a] each contains a pyridinium acceptor and dicyano-methanide donor, along with multiple biaryl dihedral twists introduced by strategically positioned *o*-methyl substituents. Single-crystal X-ray diffraction studies are performed on each chromophore to provide solid-state geometrical information. The effect of substituting a tri-*o*-methylbiaryl twisted fragment for the more difficultly prepared tetra-*o*-methylbiaryl moiety is assessed and shown to enforce similar large twist angles across the chromophore family. Also, the positioning of the sterically twisted juncture in the molecule is explored, and proximity to the donor and acceptor termini is found to be essential for enhanced NLO response. Solution-phase molecular properties are then studied using cyclic voltammetry and concentration-dependent optical absorption spectroscopy, as well as diffusion NMR spectroscopy to understand how aggregation of these dipolar zwitterions might affect the linear/nonlinear response. The results are then compared with the solid-state X-ray diffraction data to provide chromophore metrical parameters and quantitative information on actual states of aggregation in

Scheme 2. Synthesis of Twisted Chromophores 2TTMC and 4TTMC[a]
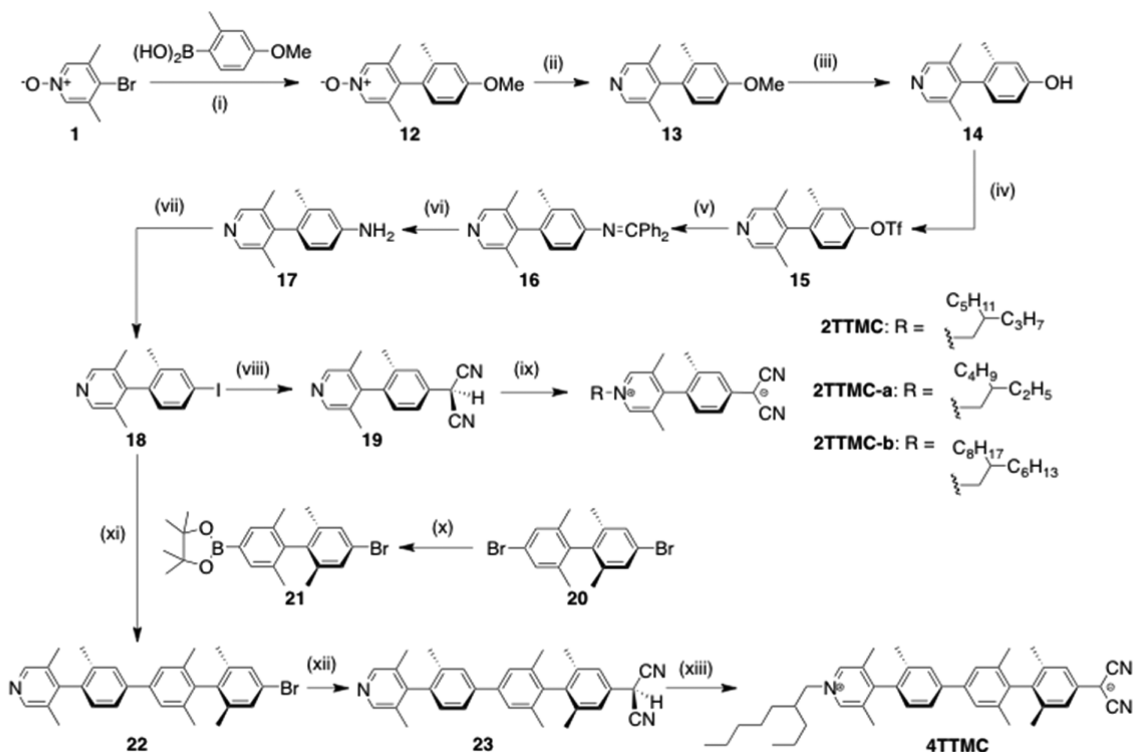
[a]Reagents and conditions: (i) Pd$_2$(dba)$_3$/Sphos, Ba(OH)$_2$, toluene; (ii) NaH$_2$PO$_2$, Pd/C, AcOH; (iii) pyridineH$^+$Cl$^-$; (iv) Tf$_2$O, pyridine; (v) HN═CPh$_2$, Pd(OAc)$_2$/BINAP, Cs$_2$CO$_3$, THF; (vi) NH$_2$OHHCl, NaOAc, MeOH; (vii) NO$^+$BF$_4^-$, CH$_3$CN, NaI; (viii) NaCH(CN)$_2$, Pd(PPh$_3$)$_4$, DME; (ix) ROTf, CH$_2$Cl$_2$, MeONa, MeOH; (x) 1.6 M *n*-BuLi, 1.5 equiv C$_9$H$_{19}$BO$_3$; (xi) Pd(PPh$_3$)$_4$, Aliquat 336, NaCO$_3$, toluene/water; (xii) NaCH(CN)$_2$, Pd(PPh$_3$)$_4$, DME; (xiii) C$_{10}$H$_{21}$OTf, CH$_2$Cl$_2$, MeONa, MeOH.

solution. Molecular hyperpolarizabilities are then evaluated by solution-phase EFISH spectroscopy. Structural and solution/solid aggregation effects are also investigated in **2TTMC** analogues by varying alkyl chain substitution. Finally, quantum calculations are performed to understand the hyperpolarizability changes induced by ring catenation, twist steric effects accompanying methyl deletion, and twisted biaryl location in the molecules.

Chromophore Synthetic Strategy. Routes to the present chromophore series are summarized in Schemes 1 and 2. The highly encumbered tetra-*o*-methylbiaryl core **2** is first synthesized via Suzuki cross-coupling of 4-bromopyridine *N*-oxide (**1**) and 2,3,5,6-tetramethylbenzene boronic acid using a Pd/dicyclohexyl(2-phenanthren-9-ylphenyl)phosphine (DCPPP) catalyst.[19] Biaryl *N*-oxide **2** is then brominated *para* to the sterically-encumbered position to afford bromobiaryl *N*-oxide **3** using a FeCl$_3$ catalyst. To complete the three-member arene system with an additional sterically encumbered twist element, a subsequent Suzuki cross-coupling of **3** and 2-methyl-4-methoxybenzene boronic acid, is accomplished using a different phosphine ligand system than used for the synthesis of **2**. Note that previous tictoid chromophores were synthesized here using Buchwald's Suzuki coupling procedure for assembling tetra-*o*-methylbiaryl fragments.[2a,19] Since this approach is typically associated with modest yields and high ligand costs, an alternative was sought to achieve the required twist angles, hence comparable hyperpolarizabilities (*vide infra*), by introducing tri-*o*-methylbiaryl fragments. This strategy was guided by computation and is discussed in detail in the Computational Results section. This approach is first demonstrated in the synthesis of **4**, which is achieved in significantly higher yield (64.1%) than was **2**, in part due to less encumbered reagents and a more active catalyst, Pd/2-dicyclohexylphosphino-2′,6′-dimethoxybiphenyl (Sphos).[19] Tris-arene pyridine *N*-oxide **4** was next quantitatively reduced to pyridine **5** using Pd-catalyzed hydrogenation with sodium hypophosphite.[33] Subsequent cleavage of the intermediate **5** methoxy group with pyridineH$^+$Cl$^-$ afforded the pyridylphenol intermediate **6**. Phenol **6** was then converted to triflate **7**, followed by the Pd-catalyzed coupling[34] of **7** with benzophenone imine, affording diphenyl ketimine **8** in 96.5% yield. Subsequent quantitative hydrolysis of **8** to primary aniline **9** was achieved using hydroxylamine hydrochloride. Triaryl iodide **10** was then obtained via diazotization of species **9** and subsequent iodination of the corresponding diazonium salt with NaI. Pd-catalyzed coupling of species **10** with sodium dicyanomethanide produced intermediate **11**, which was next regioselectively *N*-quaternized[35] with alkyl triflates, and then deprotonated to afford three-ring chromophore **3TTMC** (57.7% overall yield, Scheme 1).

Tri-*o*-methylbiaryl iodo intermediate **18** (Scheme 2) was synthesized using similar procedures, but with only one Suzuki cross-coupling reaction, without bromination. Precursor biaryl pyridine *N*-oxide **12** was synthesized in 79.7% yield from compound **1** using the same catalytic system described for **4** above. Significantly higher yields were obtained for the biaryl system versus the triaryl system in the Pd-catalyzed coupling of species **18** with sodium dicyanomethanide, affording compound **19** in 88% yield rather than 74.1% yield for **11**. The conversion of species **19** by alkylation, followed by deprotonation, produced two-ring chromophore **2TTMC** in 78% overall yield, compared to 57.7% for chromophore **3TTMC** (Schemes 1 and 2, respectively). To compare aggregation effects on the

hyperpolarizability, chromophores **2TTMC-a** and **2TTMC-b**, bearing the same backbone as **2TTMC** but with differing *N*-alkyl substitution, were prepared under similar alkylation conditions using the corresponding alkyl triflate as shown in Scheme 2.

To complete the series and enhance the yield of four-ring **4TTMC**, an alternative synthetic approach was taken. Here, instead of performing successive bromination/Suzuki coupling sequences, the sterically encumbered 4,4′-dibromo-2,2′,6,6′-tetramethyl-1,1′-biphenyl **20** was synthesized via a three-step procedure,[18] involving Zn-catalyzed reduction, hydrazine rearrangement, and subsequent bromination starting from 1-nitro-3,5-dimethylbenzene (see Supporting Information (SI) for details). Subsequent esterification of **20** by the slow addition of 1 equiv of *n*-BuLi, followed by 2-isopropoxy-4,4,5,5-tetramethyl-1,3,3-dioxaborolane addition, affords intermediate **21** in 64% yield. The central non-sterically encumbered biaryl junction was prepared via a halogen-selective Suzuki cross-coupling involving iodo derivative **18** and intermediate **21**, using Pd(PPh$_3$)$_4$ and Aliquat 336, a phase-transfer catalyst, to yield intermediate **22**. The effects of the "non-sterically" interacting twist between rings B and C of **22** (Scheme 2 and Chart 2), like the tri-*o*-methylbiaryl junctions, were verified computationally for minimal involvement in charge localization (see Computational Results section), while increasing reaction yields. Following the Pd-catalyzed coupling procedure with sodium dicyanomethanide as used in preparing the precursors to **2TTMC** and **3TTMC**, intermediate **23** was obtained, which was further alkylated and then deprotonated to afford chromophore **4TTMC** in 64% yield (Scheme 2). Each new chromophore was fully characterized via conventional analytical/spectroscopic techniques, including multi-nuclear NMR spectroscopy, mass spectrometry, and elemental analysis (see SI for synthetic details and characterization data).

Chromophore Chemical Stability. The **TTMC** chromophores exhibit somewhat different chemical stability characteristics versus the **TMC** counterparts. The **TTMC** chromophores exhibit moisture sensitivity in the decreasing order **4TTMC** > **3TTMC** ≫ **2TTMC**, rendering **3TTMC** and **4TTMC** difficult to purify by conventional chromatography, presumably reflecting the enhanced basicity of the Ar═C(CN)$_2$ group in zwitterions of increasing molecular length and charge concentration. A moisture sensitivity test of **3TTMC** in DMSO-d_6 supports the chromatographic observations (Figure 1). The phenylene ring protons adjacent to the dicyanomethanide functionality (protons a, b, and c, Figure 1) are displaced significantly downfield after exposing the solution to ambient atmosphere for 5 days. Moreover, intentional acidification shifts the equilibrium further to the protonated form (Figure 1A→D). There is a decrease in aromatic proton signals a, b, and c, and a slight upfield shift of the pyridinium peak, typical of zwitterionic character loss in these twisted chromophores. This marked proton affinity is consistent with a twisted zwitterion description of separated, non-communicating dicyanomethanide and pyridinium fragments. Kang et al. observed similar proton affinity for the **TM** chromophores containing phenoxide anions during chromatography.[2a] In the progression **2TTMC** → **3TTMC** → **4TTMC**, the observed increase in proton affinity is consistent with the chromophore elongation and enhanced charge localization on the dicyanomethanide and pyridinium termini,[36] seen in the computational study (see Computational Results, below).
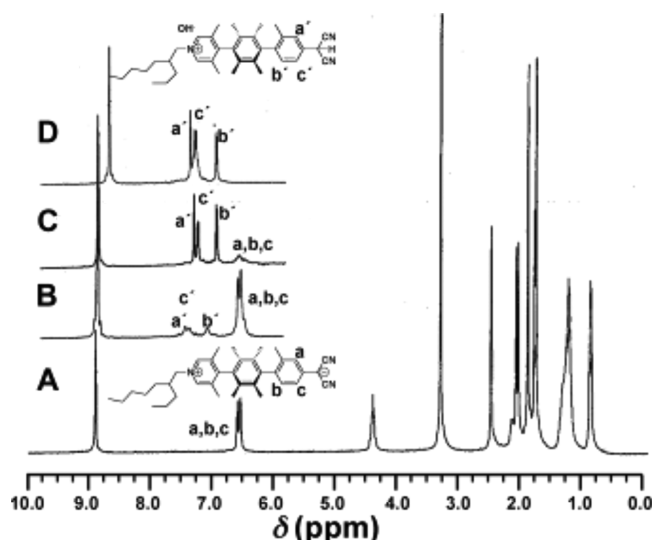
Figure 1. ^{1}H NMR spectra in DMSO-d_6 (400 MHz, 25 °C) of **3TTMC** with exposure to atmospheric moisture after 6−8 h (A), after 1 day (B), after 5 days (C), and on addition of 2% HCl solution (D). Note, these experiments were performed with exclusion of light.

Solid-State Structural Characterization. X-ray diffraction structural analyses were performed on chromophores **2TTMC**, **3TTMC**, and **4TTMC**, with single crystals obtained using solvent diffusion techniques. Crystallographic data pertaining to each determination can be found in Table S1. ORTEP drawings and selected bond lengths and inter-ring twist dihedral angles are summarized in Table 1. To achieve large twist angles and maintain charge separation with increasing molecular length, two computationally guided and synthetically expedient tactics were implemented: (1) replace tetra-*o*-methyl- with tri-*o*-methylbiaryl junctions and (2) use

standard biphenyl junctions as appropriate to achieve the desired charge separation. All of these molecules exhibit consistently large arene−arene dihedral twist angles (76−89°) except for the B−C ring juncture in **4TTMC**, where there is no *o*-arene methylation (see more below).

Using tri-*o*-methylbiaryl junctions in **2TTMC**, **3TTMC**, and **4TTMC** achieves (ring)C−C(ring) distances of 1.486(7), 1.497(4), and 1.421(6) Å, respectively, similar to typical biaryls (∼1.487 Å),[37] bimesityl (1.505(2) Å),[38] and **TMC-2** (1.488(5) Å), with any deviation in **4TTMC** likely due to charge separation effects (see below). The (ring)C−C(ring) elongation is directly related to the dihedral torsion imposed by the tri-*o*-methylbiaryl junction, giving the bond greater single σ-bond versus quinoidal character (Chart 2) as in the tetra-*o*-methylbiaryl version. For synthetic expedience, another structural feature used in this chromophore series is a biphenyl group introduced between the pyridinium (A) and phenylenedicyanomethanide (B) rings of **2TTMC** (2-rings) to yield 4-ring **4TTMC** (Chart 2). The structural data indicate a classical unfunctionalized biphenyl twist angle of 40.30°,[39] with the peripheral dihedral angles between rings A−B and C−D of 76.62 and 88.42°, respectively (**4TTMC**; Chart 2 and Table 1). Computation indicates that the inserted unfunctionalized phenylene has minimal impact on the hyperpolarizability compared to the fully methylated derivative (see below).

In addition to sterically induced substituent effects (**2TTMC** vs **TMC-2**), informative structural variations are also observed in the progression **2TTMC** → **3TTMC** → **4TTMC**, where catenation of the molecular backbone appears to enforce deconjugation/charge separation. Here, phenylene insertion reduces the *average* chromophore (ring)C−C(ring) bond length from 1.486 Å (two rings: **2TTMC**) to 1.447 Å (four-rings: **4TTMC**), still markedly greater than typical quinoidal structures with (ring)C=C(ring) ≈ 1.349 Å.[37] The contraction in (ring)C−C(ring) bond length on going from **2TTMC** to

Table 1. ORTEP Drawings of the Molecular Structures and Selected Metrical Parameters for Twisted π-Electron Chromophores 2TTMC, 3TTMC, and 4TTMC and First-Generation Chromophores TM-N, TM-1, and TMC-2

Twisted chromophore	Structure[a]	(ring)C–C(ring) (Å)[b]	(ring)C–C(CN)$_2$ (Å)	Dihedral angle[c]
TM-N[2a]		1.4932(18)	–	85.7
TM-1[2a]		1.489(2)	–	86.9
TMC-2[2a]		1.488(5)	1.463(5)	89.6
2TTMC		1.486(7)	1.454(6)	78.41
2TTMC-a		1.482(4)	1.452(4)	85.73
3TTMC		1.483(3), A–B 1.497(4), B–C	1.471(4)	86.01, A–B 84.43, B–C
4TTMC		1.421(6), A–B 1.466(5), B–C 1.453(5), C–D	1.448(6)	76.62, A–B 40.30, B–C 88.42, C–D

[a]Drawn with 50% probability ellipsoids. H atoms and solvent molecules are omitted for clarity. Ring labeling scheme (A, B, C, D) given in Chart 2. [b]Inter-ring bond distances from pyridinium cation (ring A) to dicyanomethanide anion (ring C or D), Chart 2. [c]Average dihedral angles in the respective crystal structures between rings A−B, B−C, and C−D.

4TTMC by 0.039 Å is in the 0.059 Å contraction range observed by Kang et al. in the twisted junction of synthetic intermediate **TM-N** on conversion to the corresponding zwitterion. Contraction and reduced twist angle with phenylene catenation coincides with charge separation increases between pyridinium N atom and the dicyanomethanide C center in the progression **2TTMC→4TTMC** (Table 1).

As noted for the **2TTMC**, **3TTMC**, and **4TTMC** (ring)C–C(ring) distances, the phenylene-diacyanomethanide fragments display a markedly different bond length pattern than in typical TCNQs (Table 1).[37,40] The present (aryl)C–C(dicyanomethanide) distances lack the typical TCNQ (aryl)C=C(CN)$_2$ exocyclic character ($\sim$1.392 Å),[37] and bond lengths are more in line with average **TMC** distances of 1.45 Å (Table 1).[2a] This indicates substantial negative charge localization on the $-$C(CN)$_2$ group, also evident from the observed C–CN bond shortening (1.397(3)–1.412(3) Å in **2TTMC**; 1.390(2)–1.400(4) Å in **3TTMC**; and 1.362(4)–1.368(5) Å in **4TTMC**) vs 1.427 Å in typical TCNQs,[32] as well as C≡N bond elongation (1.151(3)–1.163(4) Å in **2TTMC**; 1.152(4)–1.158(3) Å in **3TTMC**; and 1.145(3)–1.148(5) in **4TTMC**), versus 1.144 Å in typical TCNQs.[37] Finally, there is significant pyridinium aromatic character in the **TTMC** chromophores with average pyridinium C–C bond lengths of 1.366, 1.365, and 1.345 Å, respectively, for **2TTMC**, **3TTMC**, and **4TTMC**, paralleling those of N-methyl-4-phenylpyridinium salts[41] rather than those of cyclopentadienylidene-1,4-dihydropyridines.[42] Consistent with the aforementioned (ring)C–C(ring) distances, the pyridinium average bond lengths exhibit progressive decreases with chromophore catenation, further arguing for charge-separated **TTMC** ground states with slight increases in quinoidal character (Table 1) due to selective o-methyl deletion.

Solid-state packing diagrams of chromophores **2TTMC**, **3TTMC**, and **4TTMC** are shown in Figure 2. All of the present zwitterions crystallize in antiparallel pairs similar to those of **TMC-2**,[2a] presumably a result of intermolecular electrostatic interactions[43] involving the large dipole moments (see Table 4). **2TTMC** crystallizes as centrosymmetric dimeric pairs aligned in the c axis direction with two molecules of CH$_2$Cl$_2$ positioned between them (Figure 2A). Chromophore **2TTMC** has the largest π–π cofacial distance between the aromatic backbones, 8.665 Å, which is slightly larger than that in **TMC-2** (average π–π stacking distance $\approx$ 8.232 Å), possibly due to the presence of the CH$_2$Cl$_2$ molecules (Figure 2A).[2a] This distance is considerably larger than the sum of van der Waals radii between planar cofacial π-electron systems ($\sim$3.50 Å),[43] and it is likely that the bulky pyridinium N-alkyl chains contribute to the large interplanar spacings. In accordance with the increasing charge localization and structural changes observed in the **TTMC** series crystal structures, antiparallel packing is also observed in **3TTMC** and **4TTMC** where dicyanomethanide groups are proximate to the pyridinium fragment of an adjacent molecule (Figure 2B,C). As can be seen in Figure 2A–C, with an increase in backbone length and concurrent increase in dipole moment from **2TTMC** to **4TTMC**, there is also a contraction in interplanar π–π distances, from 8.665 Å (**2TTMC**), to 7.883 Å (**3TTMC**), to 7.361 Å (**4TTMC**). Additionally, CH$_2$Cl$_2$ molecules are also found to co-crystallize among the **4TTMC** dimer pairs. Thus, both intra-chromophore metrical parameters and packing distances indicate that the twisted arene units effectively localize charge and increase the dipole moments. These observations are seen to be in
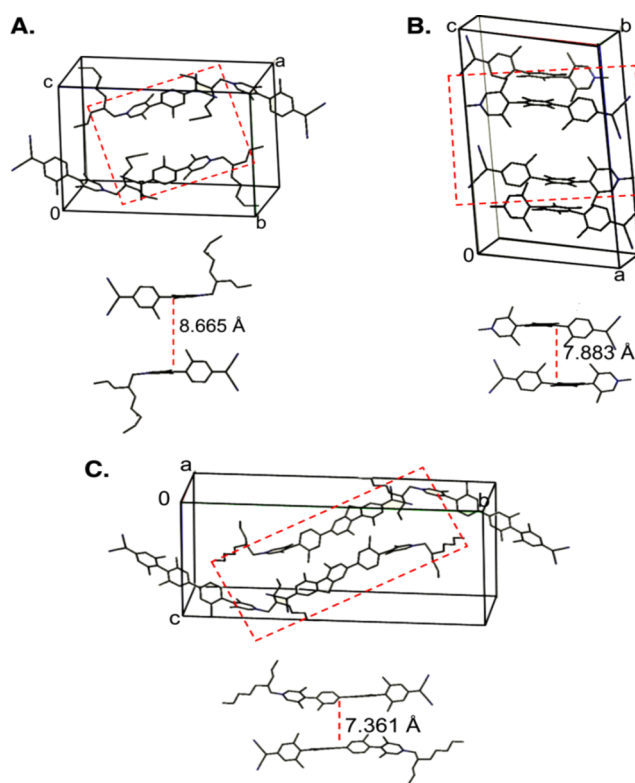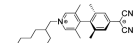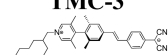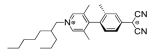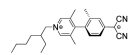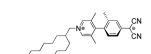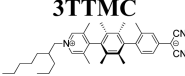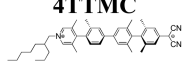

Figure 2. Crystal packing diagrams of chromophores **2TTMC** (A), **3TTMC** (B), and **4TTMC** (C). A single dimeric unit is indicated by the dashed boxes. Solvent molecules (A–C), protons (A–C), and the N-alkyl chain (B) are removed for clarity.

agreement with spectroscopic and electronic structure computational data (see Computational Results, below).

Optical Spectroscopy. Compared to the **TMC** series, the **TTMC** chromophores have relatively weak UV–vis region absorption and no noticeable features in the near-IR.[2a,14c] Previously it was reported that the twisted styrenic chromophore **TMC-3** (Chart 2) exhibits molar absorptivities as high as 38 400 M^{-1} cm^{-1}, with maximum extinction coefficients reaching $\sim$18 000 M^{-1} cm^{-1} for phenylene and pyridinium intra-subfragment excitation and $\sim$3000 M^{-1} cm^{-1} for inter-subfragment CT excitation.[2a,13] For the present series, especially **3TTMC** and **4TTMC**, the weak CT band absorption (extinction coefficients as low as 40 M^{-1} cm^{-1}) is consistent with reduced inter-ring π-conjugation and loss of a styrenic π-system versus **TMC-3** (Table 2, Figure 3A).

TTMC optical properties were studied in a range of solvents of varying polarity, similar to those used for the **TMC** series. Substantial solubilities in CH$_2$Cl$_2$ allow concentration-dependent studies of **2TTMC**, **3TTMC**, and **4TTMC** (Figure 3B–D). The normalized optical absorption spectra of the **TTMC** family in CH$_2$Cl$_2$ are shown in Figure 3A. Note that, with the exception of **2TTMC**, most of the chromophore absorption is at relatively high energies, reflecting the twisted π-systems. **2TTMC** has two high-energy peaks tentatively assigned to phenyl and pyridinium subfragment intra-ring excitations at λ_{max} = 276 nm (ε = 1852 M^{-1} cm^{-1}) and λ_{max} = 313 nm (ε = 3580 M^{-1} cm^{-1}), respectively, and a lower-energy inter-subfragment CT excitation at λ_{max} = 560 nm with a smaller oscillator strength (ε = 1040 M^{-1} cm^{-1}).[13] Introduction of a durene subfragment into the **2TTMC** backbone yields **3TTMC**, with two major spectral changes (Figure 3A,C).

Table 2. Optical Absorption Data, Optical Gap E_g, and Redox Potentials versus SCE (V) for TMC and TTMC Chromophore Series

Chromophore	$\lambda_{max}\,(\varepsilon)^c$		$E_{gap}{}^d$	E^e	
	MeOH	CH$_2$Cl$_2$	CH$_3$CN	E_{ox}	E_{red}
TMC-2	297[a] 451[b]	314(27200)[a] 569(1840)[b]	1.95	0.39	-1.56
TMC-3	397[a]	433(38400)[a] 540(2090)[b]	1.7	0.20	-1.50
2TTMC	295[a] 447[b]	276(1852)[a] 313(3580)[a] 560(1040)[b]	1.86	0.36	-1.50
2TTMC-a	296[a] 447[b]	276(9710)[a] 313(27386)[a] 561(5147)[b]	–	–	–
2TTMC-b	296 448	276(9544)[a] 313(23431)[a] 561(4164)[b]	–	–	–
3TTMC	324[a]	280(9880)[a] 310(13648)[a] 468(317)[b]	1.75	0.32	-1.43
4TTMC	254[a]	274(17466)[a] 297(14533)[a] 430(284)[b] 525(219)[b] 695(49)[b]	1.67	0.24	-1.43

[a]Assigned to intra-subfragment excitation. [b]Assigned to low-energy inter-subfragment charge-transfer excitation. [c]Optical absorption (nm) and extinction coefficient (M^{-1} cm^{-1}). [d]Estimated HOMO−LUMO gap from oxidation/reduction data (eV). [e]Redox potentials referenced to the ferrocene internal reference $E_{1/2}$ = 0.43 V versus SCE in CH$_3$CN.

First, in the high-energy region, there is a change in oscillator strength of the assigned phenyl and pyridinium subfragment excitations. Addition of another phenylene subfragment in the structure, increases the absorption in the phenylene region (λ_{max} = 280 nm, ε = 9880 M^{-1} cm^{-1} vs that of **2TTMC** (λ_{max} = 276 nm, ε = 1852 M^{-1} cm^{-1}). There is also increased oscillator strength in the pyridinium region (λ_{max} = 310 nm, ε = 13648 M^{-1} cm^{-1}; Figure 2A).[13] Furthermore, due to the effective deconjugation from the phenylene ring in **3TTMC**, Figure 3A reveals a large intensity fall and a 92 nm blue-shift in the **3TTMC** inter-fragment CT excitation (λ_{max} = 468 nm, ε = 317 M^{-1} cm^{-1} vs **2TTMC** (λ_{max} = 560 nm, ε = 1040 M^{-1} cm^{-1}; Figure 3A and Table 2).

Incorporating yet another phenylene ring in the molecular backbone, **4TTMC** induces a further increase in the phenylene and pyridinium subfragment excitation energies, with subtle changes in the lower-energy absorption region versus **3TTMC** (Figure 2C,D and Table 2). The molar absorptivity of **4TTMC** nearly doubles, with extinction coefficients of ε = 17 466 M^{-1} cm^{-1} at λ_{max} = 274 nm, and ε = 14 533 M^{-1} cm^{-1} at λ_{max} = 297 nm for the phenylene and pyridinium subfragment excitations, respectively. Compared to analogous excitations in **3TTMC**, there is also a reversal in the molar absorptivity of the phenylene- and pyridinium-centered absorptions, with the phenylene subfragment now exhibiting the greatest oscillator strength. At lower energies, there are three primary absorptions

at wavelengths >400 nm, assignable to inter-subfragment CT excitations in addition to high-energy absorptions (Figure 3D). One feature, at λ_{max} = 430 nm (ε = 284 M^{-1} cm^{-1}), is assigned to a non-twisted biaryl fragment excitation (rings B and C; Chart 2). At even lower energy, the overlapping peak at λ_{max} = 525 nm (ε = 219 M^{-1} cm^{-1}) may be an inter-subfragment excitation between phenyldicyanomethanide and another phenylene ring. As for the 695 nm (ε = 49 M^{-1} cm^{-1}) feature, it can be attributed to inter-subfragment CT excitation (Figure 3A,D). This CT excitation exhibits the lowest oscillator strength of the series, paralleling the other molar absorptivity decreases with increased molecular length.

In addition to these observations, a concentration-dependent optical analysis of chromophore **2TTMC** indicates solution-phase aggregation in moderately polar CHCl$_3$ (ε_r = 4.81; Figure 3B), as previously reported for **TMC-2**.[2a] However, unlike the **TMC-2** optical study, which was carried out over a broader range of concentrations, **2TTMC** concentrations below 10^{-5} M are uninformative due to the low molar absorptivities. Nevertheless, the **2TTMC** spectra at highest dilution can be ascribed to an essentially monomeric chromophore with a CT band centered at 603 nm (in **TMC-2** this feature is at 621 nm). Upon increasing the concentration, the spectra show diminution of this band and concomitant appearance/growth of a new transition at shorter wavelengths, suggesting the onset of aggregation.[2a,43] The well-defined isosbestic point in Figure
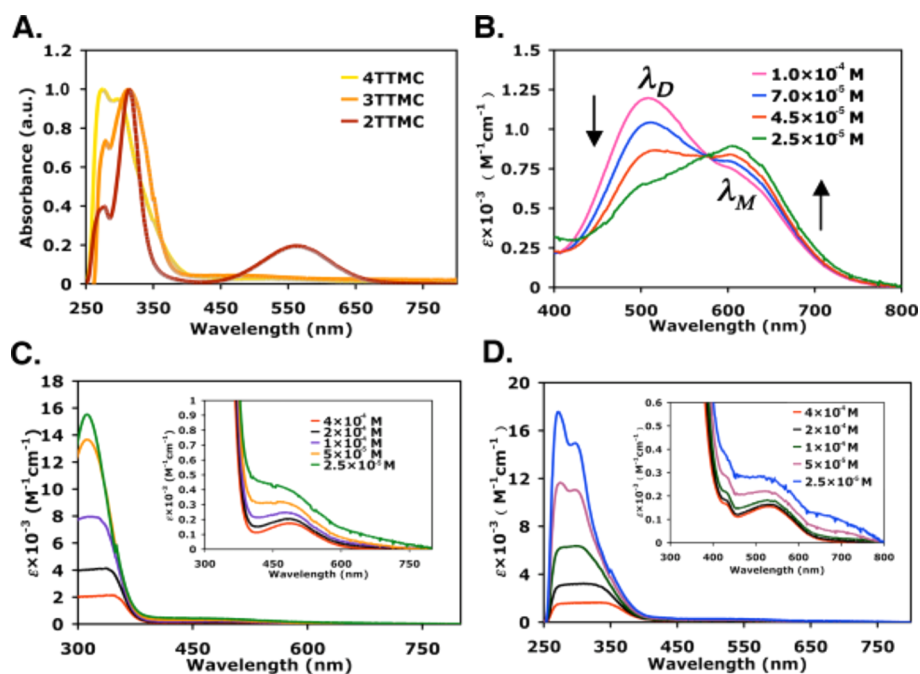
Figure 3. (A) Optical absorption spectra of **TTMC** chromophores in CH_2Cl_2. (B) Concentration-dependent **2TTMC** optical spectra in $CHCl_3$ solutions. Arrows indicate changes in CT bands upon the dilution from 1.0×10^{-4} to 2.5×10^{-5} M ascribed to a monomer−dimer/aggregate equilibrium. (C) **3TTMC** concentration-dependent changes in optical absorption in CH_2Cl_2. (D) **4TTMC** concentration-dependent changes in optical absorption in CH_2Cl_2.

3B is consistent with equilibrium between monomer and what is presumably a dimer. Similar concentration-dependent spectra in $CHCl_3$ are observed for **2TTMC-a** and **2TTMC-b** (for details, see SI, Figures S1 and S2). The aggregation states of the three two-ring twisted chromophores were investigated using the simple dimerization model $(2M = D)$ of eq 4,[2a] where K is

$$\varepsilon(c_0) = \frac{\sqrt{1 + 8Kc_0} - 1}{4Kc_0}(\varepsilon_M - \varepsilon_D) + \varepsilon_D \qquad (4)$$

the dimerization constant, ε_M and ε_D are the corresponding extinction coefficient for monomeric and dimeric chromophores, respectively. Fitting each wavelength in the ranges of 445−530 and 585−690 nm yields an average $K = 28\,300 \pm 300$ M^{-1} for **2TTMC-b**, 6700 ± 400 M^{-1} for **2TTMC**, and $12\,200 \pm 300$ M^{-1} for **2TTMC-a**. The tendency to aggregate with longer alkyl substitution in less polar chloroform ($\varepsilon_r = 4.81$) was also reported for tetraalkylated (alkyl = hexadecyl and octadecyl) calix[4]arene ethers.[44] The present aggregation mode is undoubtedly due to $\pi-\pi$ stacking facilitated by the long lipophilic alkyl chain substituents.

In addition to the concentration-dependent **2TTMC** optical spectroscopic study, the spectrum of each chromophore was examined as a function of solvent polarity (Figure 4). Note that the **2TTMC** CT bands exhibit a strong negative solvatochromic response—large blue shifts with increasing solvent polarity (in the concentration range where aggregation is insignificant). The **2TTMC** solvatochromic shift from $CHCl_3$ to MeOH is ~156 nm to higher energy (Figure 4A), comparable to the largest solvatochromic effects reported for betaine,[45] merocyanine,[SI,15b,46,47] and **TMC-2** large β chromophores (~153 nm).[2a] From the conventional interpretation,[47] negative solvatochromism indicates that the magnitude of the dipole moment in the excited electronic state is significantly smaller than that in the
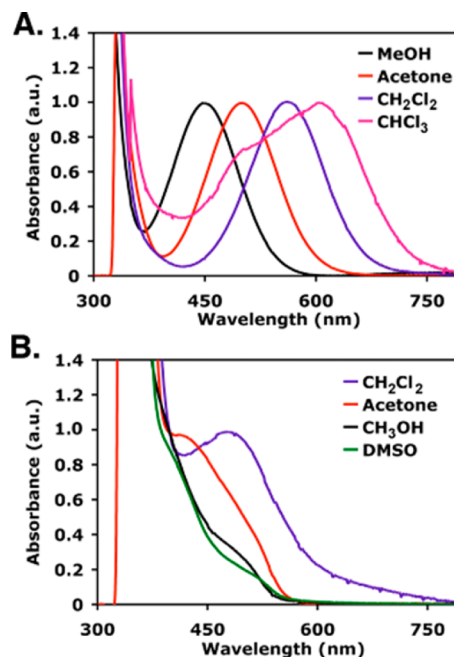

Figure 4. (A) Optical absorption spectra of **2TTMC** in solvents of different polarity. Only inter-fragment CT bands are shown here. (B) Optical absorption spectra of **3TTMC** interfragment optical excitations in solvents of varying polarity.

ground state, as also concluded for **TMC-2** and **TMC-3**.[2a] Although other factors can affect the sign of solvatochromism (e.g., aggregation, different solvent polarizabilities),[48−51] in the present case, negative solvatochromism argues that the **2TTMC** ground state is best approximated by the zwitterionic limit.[2a] Note that $CHCl_3$ was not used here due to **3TTMC** solubility limitation. Because of the breadth of the phenylene

and pyridium subfragment high-energy excitations, resolution of the MeOH and DMSO shifts, which qualitatively evidence similar negative solvatochromic shifts, is not possible (Figure 4B). Regarding **4TTMC**, the weak, low-energy excitations (Figure 3A,D) and strong overlapping absorptions of the aromatic subfragments largely obscure the negative solvatochromic shifts, which are only apparent in the disappearance of these weak excitations on going from MeOH to CH_2Cl_2. Limited chromophore solubility precluded a more diverse solvent study.

Electrochemistry. Cyclic voltammetry (CV) was carried out under N_2 in 0.1 M Bu_4NPF_6 anhydrous MeCN solutions with scanning rates of 60−150 mV/s. Voltammograms of ~10^{-3} M CH_3CN solutions evidence the charge-richness engendered by twisted biaryls. Although precise E_{gap} determination requires knowledge of the standard potentials, HOMO−LUMO gaps can be estimated from the present oxidative/reductive data to be ~1.86, ~1.75, and ~1.67 eV for **2TTMC**, **3TTMC**, and **4TTMC**, respectively, and are in good agreement with the optical bandgaps derived from optical absorption spectroscopy (Table 2). In comparison to chromophores **TMC-2** and **TMC-3**, the present series exhibits similar HOMO−LUMO gaps (Table 2). Note that there is a systematic contraction in these gaps with increasing phenylene catenation in the **2TTMC** → **3TTMC** → **4TTMC** series. This is consistent with π-system extension, and presages, according to the two-level model, a concurrent increase in hyperpolarizability (β) from **2TTMC** → **3TTMC** → **4TTMC**.

4TTMC Aggregation by Diffusion NMR Spectroscopy. Diffusion NMR is a powerful tool to obtain quantitative information on molecular dimensions and intermolecular aggregation[52] in solution. Translational self-diffusion coefficients of **4TTMC** as a function of concentration were measured at 295.7 K in CD_2Cl_2 and DMSO. From D_t values, the hydrodynamic dimensions of **4TTMC**, assumed to have ellipsoidal shapes, were derived by applying the modified Stokes−Einstein equation (eq 5),[53] where k is the Boltzmann

$$D_t = \frac{kT}{fc\pi\eta\sqrt[3]{abd}} \qquad (5)$$

constant, T is the absolute temperature, η is the fluid viscosity, c is the size factor, which depends on the ratio between the solvent radius and that of the diffusing particle, and f is the shape factor, which depends on the values of the ellipsoid semi-axes (a, b, and d, with $a > b > d$).[54] Structure parameter P (= $kT/\pi\eta D_t = fc(abd)^{1/3}$) is derived from the known values of η and T and the measured D_t values (Table 3).

The aggregation numbers N (the average number of monomer units in an aggregate), calculated via eq 8 (see below) significantly diverge from unity (Table 3), indicating that **4TTMC** undergoes self-aggregation in CD_2Cl_2. Assuming that (1) self-aggregation is limited to a monomer−dimer equilibrium and (2) monomer and dimer possess ellipsoidal shapes, the dimerization equilibrium constant (K_D) can be estimated by fitting the experimental trends of P versus C with eq 6, where x_M and x_D are the mole fractions of the monomer and dimer, respectively.

$$P = x_M P_M + x_D P_D \qquad (6)$$

x_M and x_D can then be expressed as functions of K_D and C (eq 7):[53]

Table 3. Diffusion Coefficients ($10^{10}D_t$, m^2 s^{-1}), P Values (Å), and Aggregation Numbers (N)[a] for the Chromophore 4TTMC as a Function of Concentration (C, mM) and Solvent

entry	solvent	C	D_t	P	N
1	CD_2Cl_2	0.027	6.89	45.63	1.28 ± 0.05
2	CD_2Cl_2	0.16	6.30	49.95	1.55 ± 0.06
3	CD_2Cl_2	0.18	6.06	51.90	1.57 ± 0.06
4	CD_2Cl_2	0.56	5.93	53.01	1.71 ± 0.04
5	CD_2Cl_2	0.76	5.54	56.71	1.74 ± 0.04
6	CD_2Cl_2	0.98	5.77	54.47	1.77 ± 0.04
7	CD_2Cl_2	2.00	5.52	56.93	1.83 ± 0.03
8	CD_2Cl_2	6.15	5.35	58.76	1.90 ± 0.02
9	DMSO	0.057	1.66	38.09	
10	DMSO	0.57	1.60	39.54	
11	DMSO	1.48	1.56	40.46	

[a]Calculated according to eq 8. The error intervals on N are reported at 95% confidence.

$$x_M = 2 - \frac{2C}{C + \frac{\sqrt{1 + 8K_D C} - 1}{4K_D}} \quad \text{and}$$

$$x_D = -1 + \frac{2C}{C + \frac{\sqrt{1 + 8K_D C} - 1}{4K_D}} \qquad (7)$$

Parameters P_M and P_D depend on the ellipsoid semi-axes (a_M, a_D, b_M, b_D, d_M, d_D) and the hydrodynamic radius of the solvent (r_{solv}). The latter can be considered approximately equal to the van der Waals radius of CD_2Cl_2 (r_{solv} = 2.49 Å). Monomeric **4TTMC** is treated as a prolate ellipsoid ($a > b = d$) having the major semi-axis (a_M) equal to 15.2 Å (ca. half the distance between the terminal CH_3 group and the N of the CN moiety in the conformer having a fully elongated alkyl chain, Figure 5).
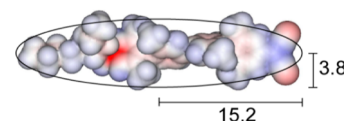

Figure 5. Monomer van der Waals surface of the **4TTMC** chromophore. The ellipsoid used as geometrical models for diffusion NMR data analysis is depicted in black.

The minor semi-axis ($b_M = d_M$ = 3.8 Å) is derived from the experimentally determined P_M value in DMSO (38.09 Å), using eq 5, assuming that only monomers are present in such a polar solvent at the lowest investigated concentration (0.057 mM).

Having estimated a_M and b_M, we can derive the theoretical value of P_M in CD_2Cl_2 (39.04 Å). Experimental P data in CD_2Cl_2 as a function of concentration are then fitted using eq 6 (Figure 6), in which K_D and P_D are the unknowns. The best fit gives K_D = 26 000 ± 8300 M^{-1} and P_D = 60.54 ± 1.12 Å. The dimerization equilibrium constant of **4TTMC** in CH_2Cl_2 is approximately 100 times larger than that of **TMC-2** (203 ± 330 M^{-1} from diffusion NMR[14c] and 243 ± 30 M^{-1} from concentration-dependent optical absorption studies[2a]). From the K_D value, aggregation numbers (N) can be computed at each concentration according to eq 8 (Table 3). Assuming that **4TTMC** stacks along the major semi-axis, the two minor semi-axes (b_D and d_D) of the dimer can be easily derived: $b_D = 2b_M$ = 7.6 Å and $d_D = b_M$ = 3.8 Å. In contrast, the major semi-axis (a_D) depends on the extent of the linear overlap (L) between the
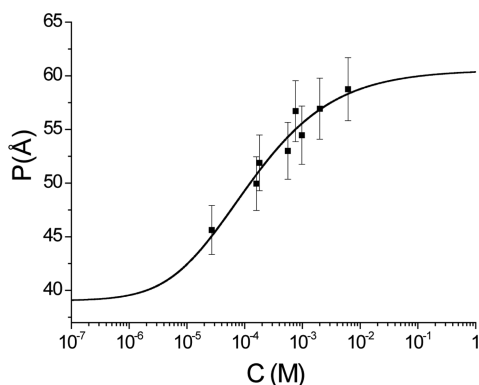
Figure 6. Experimental P values as a function of concentration for **4TTMC** in CD_2Cl_2. The solid line is the best fit to the data using eq 6.

$$ N = \frac{2C}{C + \frac{\sqrt{1 + 8K_D C} - 1}{4K_D}} \tag{8} $$

two monomers. The estimated P_D value (60.54 ± 1.12 Å) corresponds to an ellipsoidal dimer having a_D = 21.9 Å, and, consequently, $L \approx 17$ Å.
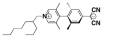
■ COMPUTATIONAL RESULTS

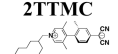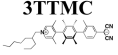Calculations were aimed at determining molecular structure parameters and hyperpolarizabilities for the **2TTMC**, **3TTMC**, **4TTMC** series as a function of (1) placement of o-methyl groups at selected skeletal positions to guide synthetic design and (2) increasing the chromophore π-expanse via incorporation of additional phenylene units. As a test case, a tri-o-methyl version of **TMC-2**, **2TTMC**, was designed, computationally analyzed, and ultimately found to exhibit promising structural and response features (Table 4). The computed ground-state arene−arene twist angles for **TMC-2** and **2TTMC**

differ by ∼1° in the gas phase, with a minimal change in computed (ring)C−C(ring) and (ring)C−C(CN)$_2$ bond lengths. This result is in good agreement with the crystal structure metrical parameters (Tables 1 and 4). Moreover, in keeping with similar dihedral angles, the ground-state dipole moments (μ_g) of both chromophores are computed to be within 3 D. Interestingly, the hyperpolarizability is found to decrease slightly upon the removal of the fourth o-methyl group (**TMC-2→2TTMC**). As expected from the two-level model, a slight reduction in twist angle should effect only a minimal increase in energy separating the zwitterionic ground state and the first excited state (ΔE_{ge}), a decrease in the dipole moment change ($\Delta\mu_{ge}$), and a 10% fall in computed β_{vec} (Table 4). This presents only a minor compromise in response vs the 20−30% increase in overall synthetic yield obtained using the tri-o-methylbiaryl coupling vs tetra-o-methyl synthetic methodology (see Chromophore Synthetic Strategy above).

To build on the response enhancement obtained with sterically enforced biaryl twists, as found in **TMC-2**, while providing decreased absorption at longer wavelengths and photo-oxidative stability,[16] the present objective was to investigate the consequences of lengthening the chromophore π-system while isolating D/A fragments and ensuring aromatic stabilization as described above.[15] In conventional planar D−A chromophores, this is an effective strategy for increasing the magnitude of β_{vec}.[15] Similar trends are evident in considering the computed HOMO and LUMO spatial distributions for the present **TTMC** chromophores (Figure 7). The HOMO is seen to be increasingly localized on the dicyanomethylene substituent on progressing from **2TTMC** to **4TTMC**. The LUMO exhibits an opposite trend with increasing localization on the pyridinium cation. In this progression, phenylene ring addition effects pronounced changes in dipole moment ($\Delta\mu_{ge}$), transition dipole matrix elements (μ_{ge}), and optical excitations (ΔE_{ge})—all important within the two-level model, as discussed earlier.

Table 4. Computed Chromophore Structural and Electronic Structural Properties (at the B3LYP and INDO/SCI Levels) Associated with Increasing Chromophore Length and Charge Separation in the TICT Chromophore Series 2TTMC, 3TTMC, 4TTMC versus Previous Generation TMC-2

Chromophore	ΔE_{ge} (eV)	μ_g (Debye)	$\Delta\mu_{ge}$ (Debye)	β_{vec}	twist angle (deg)[a]	(ring)C−C(ring) (Å)[b]	(ring)C−C(CN)$_2$ (Å)
TMC-2	2.45	29.8	-21.4	518	68	1.468	1.426
2TTMC	2.48	26.5	-19.2	465	67	1.464	1.423
3TTMC	1.68	51.3	-44.3	6,380	68 (A−B) / 67 (B−C)	1.458 (A−B) / 1.461 (B−C)	1.418
4TTMC	1.42	74.0	-63.2	11,078	67 (A−B) / 35.8 (B−C) / 68 (C−D)	1.453 (A−B) / 1.467 (B−C) / 1.446 (C−D)	1.413
4TTMC′[c]	1.41	77.8	-63.4	11,534	67 (A−B) / 67 (B−C) / 68 (C−D)	1.453 (A−B) / 1.451 (B−C) / 1.447 (C−D)	1.414

[a]Arene−arene torsional angles between indicated chromophore arene rings (Chart 2). [b]Corresponding arene−arene juncture bond distances between indicated chromophore arene rings (Chart 2). [c]Completely methylated derivative of **4TTMC**.
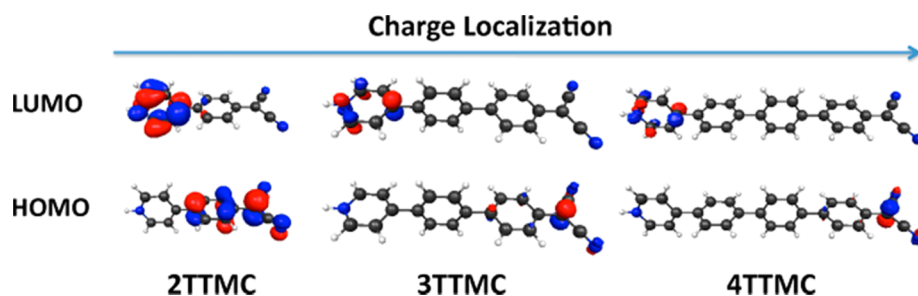
Figure 7. Isodensity surface plots of the HOMOs and LUMOs of the **TTMC** chromophores computed at the B3LYP level. Note the increasing charge localization with enforced twist angle π-system extension. In this particular case the twist angles are imposed rather than using *o*-methyl substituents.

On progressing from **2TTMC → 3TTMC → 4TTMC**, there is a 40% fall in computed excitation energy from the zwitterionic ground state to the first excited state (ΔE_{ge}), along with a concomitant threefold increase in dipole moment change ($\Delta \mu_{ge}$). These structural modifications result in a very large overall β_{vec} enhancement of ~23 times in the 2-ring → 4-ring structure change (Table 4, Figure 8). From Figure 8, note
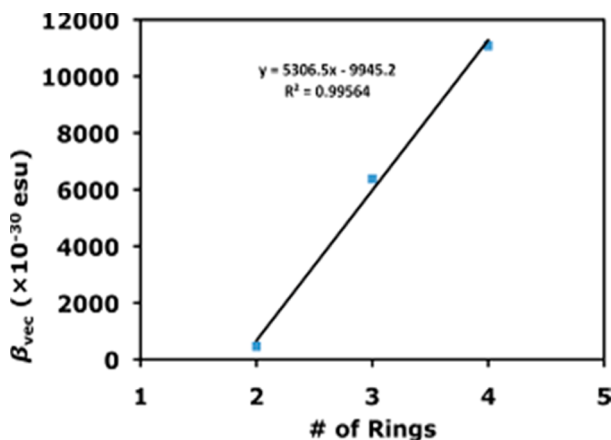

Figure 8. Computed (at INDO/SCI level) gas-phase molecular hyperpolarizability for twisted chromophores **2TTMC**, **3TTMC**, and **4TTMC**, as a function of phenylene ring extension.

that the response is approximately linear with ring catenation. Structurally, the present twist angles are comparable to those previously computed for the **TMC** systems at this computationally efficient level of theory.[2a,8a,b,13,14a,b] The only exception is **4TTMC**, where the non-methylated biphenylene fragment

between rings B and C has a computed dihedral angle of 35.8°. Importantly, these calculations show that the completely methylated derivative of **4TTMC**, **4TTMC′**, exhibits no great advantage in terms of hyperpolarizability response (Table 4).

EFISH Measurements. EFISH measurements for chromophores **2TTMC**, **3TTMC**, and **4TTMC** performed in CH_2Cl_2 and DMF at different concentrations, always give negative $\mu\beta_{vec}$ values in agreement with the solvatochromic results. For the three 2-ring TICT chromophores with varying alkyl substitutions, **2TTMC**, **2TTMC-a**, and **2TTMC-b**, an interesting $\mu\beta_{vec}$ trend is observed. In less polar CH_2Cl_2 solutions, the $\mu\beta_{vec}$ data exhibit a pronounced concentration dependence (see Table 5), due to the aforementioned aggregation effects typical of other zwitterionic chromophores.[2a,13,14] Thus, the $\mu\beta_{vec}$ of **2TTMC-a** rapidly increases as the concentration falls from 8.5×10^{-5} to 2×10^{-5} M, suggesting centrosymmetric aggregates that are progressively dissociated by lowering the concentration as in the case of **TMC-2** and **TMC-3** (Chart 2).[12] In contrast, for **2TTMC-b**, the $\mu\beta_{vec}$ values are essentially concentration-independent (the small variations observed in $\mu\beta_{vec}$ are within experimental error), in agreement with the concentration independent absorption spectra of **2TTMC-b** in CH_2Cl_2 (Figure S5) and with the presence of the sterically more encumbered alkyl substituents which are likely to more effectively suppress aggregation. The EFISH $\mu\beta$ values of **3TTMC** and **4TTMC** exhibited a large standard deviation in EFISH parameters even for relatively high concentration solutions (5×10^{-4} M), which may reflect the reactivity issues discussed in the Chromophore Chemical Stability section. Further NLO property characterization of **3TTMC** and **4TTMC** is under investigation.

Table 5. EFISH Data for Three 2TTMC Molecules with Varied Alkyl Substitution in CH₂Cl₂ Solution

Chromophore	Alkyl substitution	c (mol/L)	$\mu\beta_{vec}$ in CH_2Cl_2 ($\times 10^{-48}$ esu)
2TTMC ($C_{27}H_{35}N_3$)	R = (C₅H₁₁, C₃H₇)	8.5×10^{-5}	-6000
2TTMC-a ($C_{25}H_{31}N_3$)	R = (C₄H₉, C₂H₅)	8.5×10^{-5}	-5600
		2×10^{-5}	-10500
2TTMC-b ($C_{33}H_{47}N_3$)	R = (C₈H₁₇, C₆H₁₃)	8.5×10^{-5}	-11500
		2×10^{-5}	-10600

■ DISCUSSION

Chromophore Synthetic Strategies with Tri-*o*-Methyl-biarylene Fragments. Compared to the synthesis of **TMC-2** and other tetra-*o*-methylbiaryls, a major modification in synthesizing the present generation of tictoid chromophores was implemented to increase efficiency (Schemes 1 and 2). For the synthesis of **2TTMC**, **3TTMC**, and **4TTMC**, biaryl and tri-*o*-methylbiaryl twisted junctions were used to simplify chromophore preparation (Schemes 1 and 2). Suzuki C−C coupling methodology was employed with the highly active Pd(0)/Buchwald ligand catalyst[19] in two different synthetic modalities.[2a] The first involved Suzuki coupling of 4-bromopyridine *N*-oxide (**1**) with 4-methoxy-2-methylphenylboronic acid to produce intermediate **12** in 79.7% yield (Scheme 1). This provides a 27% increase in overall yield vs the tetra-*o*-methyl analogue synthesis.[2a] Intermediate **12** was then used in the synthesis of **2TTMC** and **4TTMC** (Scheme 2) with enhanced product yields. Using the previously reported hydrazine rearrangement[18] for the synthesis of the tetra-*o*-methylbiaryl fragment on the dicyanomethanide end of **4TTMC**, only one sterically sensitive Suzuki coupling is required. For the synthesis of **3TTMC**, unlike **2TTMC** and **4TTMC**, two successive sterically hindered Suzuki couplings must be performed in good yield. Initial synthetic attempts for **3TTMC** using two successive tetra-*o*-methylbiaryl Suzuki couplings proceeded in yields of 48% and 2%. The 2% yield was increased to 64% using 4-methoxy-2-methylphenylboronic acid instead of 4-methoxy-2,6-methyl-phenylboronic acid to afford tri-*o*-methylbiaryl intermediate **4** (Scheme 1).

TTMC Molecular Structure Characteristics. Crystallographic analyses of the target chromophores reveal consistently large and relatively uniform arene−arene dihedral twist angles (76−89°; Table 1) with the exception of the intentionally placed B−C junction (∼40°) in **4TTMC**. These suggest that the *o*-methyl substitution patterns (e.g., biaryl, tri-*o*-methylbiaryl, and tetra-*o*-methylbiaryl) provide similarly sufficient nonbonded repulsions to achieve the tictoid conformation required for substantially enhanced molecular hyperpolarizability.[13,14] Specifically, **2TTMC** and **2TTMC-a** exhibit dihedral angles of ∼78° and ∼86, only a few degrees smaller than that of **TMC-2**, plausibly sufficient for achieving a large β. In general, the location and the number of inter-ring methyl substituents in this series leads to reductions in inter-ring π-conjugation, which in turn, promotes aromatic stabilization[15] of pyridinium, phenylene, and phenylene−dicyanomethanide constituents, ultimately resulting in dominant charge-separated zwitterionic ground states. Zwitterionic structural assignments for **2TTMC** through **4TTMC** are further supported by the diffraction-derived metrical parameters, such as (ring)C−C(ring) and (dicyanomethanide)C−C(aryl) distances, along with the pyridinium and phenylene−dicyanomethanide fragments. In additional to increased charge separation, chromophore (ring)C−C(ring) bond length contractions are also observed in the progression **2TTMC → 3TTMC → 4TTMC**. These (ring)C−C(ring) contractions appear to reflect, among other factors, the deletion of methyl groups in various parts of the chromophore structures. Furthermore, the computed structures at the B3LYP level are in good agreement with the X-ray metrical parameters, identifying charge-separated zwitterionic structures as the ground states. This conclusion is further supported by the increase in the computed ground-state dipole moment (μ_g) from 26.5 to 74 D on proceeding from

2TTMC to **4TTMC** (Tables 1 and 4). Previous NMR studies showed that the **TMC-2** twist angle is essentially unchanged in solution.[10c]

Further support for the zwitterionic ground state/increased charge localization comes from solution optical spectroscopy. The chromophore spectra exhibit both inter-ring HOMO−LUMO CT excitations, as well as intra-subfragment transitions within the pyridinium and phenylene fragments, implying a tictoid ground state for **2TTMC** through **4TTMC**. From Figure 3A, in the progression from 2-rings to 3-rings to 4-rings (**2TTMC → 3TTMC → 4TTMC**), there is an observed reduction in the CT band oscillator strength, reflecting reductions in inter-ring π-conjugation. Diminution in the CT band is also accompanied by oscillator strength growth in the phenylene intra-subfragment absorption, indicative of isolated twisted rings (Figure 3A, Table 2),[13] and the strong negative solvatochromism observed for **TTMCs** indicates that the ground-state dipole moment is far greater than that in the excited state, consistent with a dominant zwitterionic ground state.[2a,11−13,15a,49] Additionally, unlike typical planar high-response D−A chromophores, the reduced absorption cross sections at wavelengths greater than 400 nm for **3TTMC** and **4TTMC** meet EO device application criteria with negligible near-IR absorption (Figure 3A,C,D).

Aggregation Trends. NLO chromophore aggregation tendencies are typically important in understanding EO response, as well as in ultimate device technologies.[1,3,51] For merocyanine dyes, centrosymmetric organization via dipole−dipole interactions is anticipated[2a] and is detrimental to EO applications in which microstructurally polar chromophore arrangement is essential. It is only by suppressing aggregation that exceptional molecular hyperpolarizabilities and bulk EO response can be realized.[3,10h,55] As expected, the present new series of TICT chromophores exhibits aggregation that is evident in the crystal structures and previously established TICT chromophore properties.[2a,12−14] The zwitterion packing in crystals features centrosymmetric antiparallel dimer formation (Figure 2). The substituent- and solvent-modulated interplanar distances between central points along the molecular axis of each dimer are significantly larger than observed in planar merocyanine zwitterion dimers (∼3.50 Å)[43] and it can be seen in Figure 2, using the same *N*-alkyl substituent (for solubility), that the minimum intermolecular distance falls from 8.665 to 7.361 Å on going from chromophore **2TTMC** to **4TTMC**. Additionally, crystallographic packing densities mirror aggregation tendencies. Thus, solid **TMC-2** has a density of 1.110 g/cm³, whereas the corresponding **TTMC** chromophores have densities ranging from 1.172 to 1.261 g/cm³, with **4TTMC** having the largest.

Further support for **TTMC** chromophore aggregation comes from the concentration-dependent optical spectra with substantial blue-shifts and falling CT excitation intensity on dilution (Figure 3B). These changes closely parallel those of **TMC-2**.[2a] The **2TTMCs** also display isosbestic points, consistent with well-defined aggregation equilibria and involving H-type antiparallel aggregates as in the diffraction data (Figures 3B, S1, and S2). Furthermore, diffusion NMR spectroscopic analysis of **4TTMC** aggregation shows good agreement with the X-ray-derived pyridinium N (where the positive charge is mainly located)−dicyanomethanide C (where the negative charge is mainly located) distance of 16.739 Å (Table S2). Thus, as in the solid state, it is reasonable to hypothesize that the dimerization process in solution is the

consequence of minimizing the distance between positive and negative charges of two adjacent chromophores.

EO Response. The present B3LYP/INDO-SOS computations provide an understanding of **TTMC**'s EO response. Previous TICT chromophore calculations helped elucidate their unique response,[12,13,14a,c,d] and the state-average complete active space self-consistent field (SA-CASSCF) formalism has provided the most accurate estimate of EO properties to date.[14c] These computations also provide insight into solvation effects on α and β. In the present work, configuration interaction with intermediate neglect of differential overlap (CI/INDO) was selected with SOS to characterize **TTMC** response trends,[13] due to the computational efficiency and qualitative agreement with experiment noted previously.[2a,13,14c] Using metrical parameters from B3LYP energy minimization, response changes can be correlated with the constituent two-level model variables in Table 4 and eq 1. In the absence of an electric field (gas phase, $F = 0.0$ au), the aromaticity resulting from sterically enforced twists is retained across the **TTMC** series. This pyridinium/phenylene resistance to charge delocalization effectively increases the ground-state dipole moment by ~3 times for **2TTMC** → **4TTMC**, with substantial charge localization evident in the HOMO−LUMO contours (Figure 7). Furthermore, a 30% fall in ΔE_{ge} accompanies this π-system extension. This computational result is in good agreement with electrochemical data, which yields estimated HOMO−LUMO gaps of ~1.86, 1.75, and 1.67 eV for **2TTMC**, **3TTMC**, and **4TTMC**, respectively (Tables 2 and 4). Gas-phase calculations on the **TTMC** series predict NLO response changes to scale nearly linearly with phenylene catenation (Figure 8), and **4TTMC** exhibits the largest computed hyperpolarizability to date, $\beta_{cal} \approx 11\,000 \times 10^{-30}$ esu, which translates into an enormous $\mu\beta \approx 900\,000 \times 10^{-48}$ esu. The estimated figure of merit, $\mu\beta/M_w$, is as high as 1500×10^{-48} esu, nearly 1.5 times larger than the very high experimental value for **TMC-3** and ~30 times larger than that in high-response planar D/A systems (Table 4).[2a,o]

Another important chromophore design criterion revealed by this study is the location and density of biaryl *o*-methyl substitution. Thus, direct comparison of **TMC-2** to **2TTMC** in both solid state and solution using computation, X-ray diffraction, and optical spectroscopy, supports their overall structural/electronic similarities (Tables 1, 2 and 4), which translate into comparable calculated β responses of 518×10^{-30} and 465×10^{-30} esu for **TMC-2** and **2TTMC**, respectively. Considering the superior synthetic efficiency of the tri-*ortho* strategy and the minimal loss in **2TTMC** response, this modification is entirely justifiable. In the 4-ring series, complete *o*-methylation in **4TTMC′** versus **4TTMC** is also computed to be unnecessary (Table 4). Calculated hyperpolarizabilities for both systems are within ±4%, demonstrating the importance of twisted biaryl charge isolation via sterically enforced twists positioned adjacent to electron donors (between rings C and D) and acceptors (between rings A and B; Chart 2). In contrast, relaxation between rings B and C (Chart 2) does not sacrifice the calculated dipole moments or hyperpolarizabilities. Thus, this structural modification enhances synthetic efficiency while increasing NLO response attributable to π-system extension.

In support of the above results, EFISH-derived $\mu\beta_{vec}$ values for chromophores **2TTMC**, **3TTMC**, and **4TTMC** in CH$_2$Cl$_2$ and DMF exhibit negative signs (Table 5), indicating, as expected from the computation and solvatochromism, that the ground state is more polar than the excited state. Importantly, EFISH of the two-ring TICT chromophores with varying alkyl substituents, **2TTMC**, **2TTMC-a**, and **2TTMC-b**, reveals molecular hyperpolarizabilities as high as -433×10^{-30} esu ($\mu\beta_{vec} \approx -11\,000 \times 10^{-48}$ esu), in accordance with the B3LYP/INDO-SOS results. Further tictoid chromophore work will focus on increasing solubility, the measurement precision, and further extending the π-systems as well as structural modification to minimize the aggregation.

■ CONCLUSIONS

A series of computationally engineered, twisted π-system multi-arylene electro-optical chromophores (**TTMCs**) was prepared and characterized. Synthetic challenges were overcome using a combination of computational design and improved methodologies. Specifically, a three-*o*-methyl group twisting strategy and Buchwald ligands for sterically hindered Suzuki couplings were introduced. For the **4TTMC** synthesis, instead of performing successive bromination/Suzuki coupling sequences, the sterically imposed twisted connections were coupled separately, followed by selective coupling to attach the donor and acceptor end groups. Crystallographic analysis of this series reveals large, nearly invariant ring−ring dihedral angles (76−88°), except for the B−C junction in **4TTMC**, enforced via either tri-*ortho*- or tetra-*ortho*-substituted biarylene cores. Sterically induced twists are only necessary at junctions proximate to donor and acceptor fragments (charged pyridinium and dicyanomethanide groups; e.g., rings A−B and C−D of **4TTMC**) to optimize zwitterionic charge separation. The extent of charge separation in the zwitterionic ground states is largely governed by twisted phenylene catenation, hence chromophore molecular length. Optical spectra reveal increasingly twist-induced reduction of inter-ring charge transfer and negative solvatochromism from **2TTMC** → **3TTMC** → **4TTMC**, again a result of the weak interaction between the twisted phenylene units. Increased phenylene intra-ring absorption and concomitant CT band reduction with molecular length also provide excellent near-IR transparency. The solution-phase optical spectroscopy and solid-state structural characterization support enhanced length-dependent zwitterionic charge separation in the **2TTMC** → **3TTMC** → **4TTMC** progression, and increased tendencies for centrosymmetric aggregation−π-stacking distances fall from 8.665 to 7.361 Å in the presence of minor reductions in inter-ring bond lengths and twist angles at select positions.

Additionally, this systematic study further supports the qualitative "two-level" model for chromophore descriptions, and shows that exceptionally large hyperpolarizabilities (β) are plausible with nonresonant $\mu\beta_{vec}$ values as high as $-900\,000 \times 10^{-48}$ esu and chromophore figures of merit, $\mu\beta/M_w$, as high as 1500×10^{-48} esu. This work shows that extended twisted π-electron species are promising candidates for EO applications and provides new insight into EO chromophore design. How far such twisted π-systems can be extended and what hyperpolarizabilities can be achieved will be the subject of future studies.

■ ASSOCIATED CONTENT

Ⓢ Supporting Information

The Supporting Information is available free of charge on the ACS Publications website at DOI: 10.1021/jacs.5b04636.

Experimental details, characterization data for new compounds, and additional results (PDF)

X-ray crystallographic data for **2TTMC** (CIF)

X-ray crystallographic data for **2TTMC-a** (CIF)

X-ray crystallographic data for **3TTMC** (CIF)

X-ray crystallographic data for **4TTMC** (CIF)

■ AUTHOR INFORMATION

Corresponding Authors

*ratner@chem.northwestern.edu

*t-marks@northwestern.edu

Author Contributions

‖Y.S. and D.F. contributed equally.

Notes

The authors declare no competing financial interest.

■ REFERENCES

(1) For recent reviews of organic electro-optics, see: (a) Liu, J.; Xu, G.; Liu, F.; Kityk, I.; Liu, X.; Zhen, Z. *RSC Adv.* **2015**, *5*, 15784. (b) Beverina, L.; Pagani, G. A. *Acc. Chem. Res.* **2014**, *47*, 319. (c) Wu, W.; Qin, J.; Li, Z. *Polymer* **2013**, *54*, 4351. (d) Dalton, L. R.; Sullivan, P. A.; Bale, D. H. *Chem. Rev.* **2010**, *110*, 25. (e) Li, Z.; Li, Q.; Qin. *Polym. Chem.* **2011**, *2*, 2723. (f) *Handbook of Organic Materials for Optical and (Opto)electronic Devices*; Perez-Moreno, J., Ostroverkhova, O, Eds.; Woodhead Publishing: Cambridge, UK, 2013. (g) Dalton, L. R. In *Handbook of Conducting Polymers*; Skotheim, T. A., Reynolds, J. R., Eds.; CRC Press LLC: Boca Raton, FL, 2007; Chapter 2. (h) *Characterization Techniques and Tabulations for Organic Nonlinear Optical Materials*; Kuzyk, M. G., Dirk, C. W., Eds.; Marcel Dekker: New York, 1998. (i) *Nonlinear Optics of Organic Molecules and Polymers*; Nalwa, H. S., Miyata, S., Eds.; CRC Press: Boca Raton, FL, 1997. (j) *Organic Nonlinear Optical Materials*; Bosshard, Ch., Sutter, K., Prêtre, Ph., Hulliger, J., Flörsheimer, M., Kaatz, P., Günter, P., Eds.; Advances in Nonlinear Optics, Vol. 1; Gordon & Breach: Amsterdam, 1995. (k) *Molecular Nonlinear Optics: Materials, Physics, Devices*; Zyss, J., Ed.; Academic Press: Boston, MA, 1994.

(2) (a) Kang, H.; Facchetti, A.; Jiang, H.; Cariati, E.; Righetto, S.; Ugo, R.; Zuccaccia, C.; Macchioni, A.; Stern, C. L.; Liu, Z.; Ho, S.-T.; Brown, E. C.; Ratner, M. A.; Marks, T. J. *J. Am. Chem. Soc.* **2007**, *129*, 3267. (b) Menezes, A. P.; Jayarama, A.; Ng, S. W. *J. Mol. Struct.* **2015**, *1088*, 85. (c) Liu, F.; Yang, Y.; Cong, S.; Wang, H.; Zhang, M.; Bo, S.; Liu, J.; Zhen, Z.; Liu, X.; Qiu, L. *RSC Adv.* **2014**, *4*, 52991. (d) Peddie, V.; Anderson, J.; Harvey, J. E.; Smith, G. J.; Kay, A. J. *J. Org. Chem.* **2014**, *79*, 10153. (e) Planells, M.; Pizzotti, M.; Nichol, G. S.; Tessore, F.; Robertson, N. *Phys. Chem. Chem. Phys.* **2014**, *16*, 23404. (f) Cabanetos, C.; Bentoumi, W.; Silvestre, V.; Blart, E.; Pellegrin, Y.; Montembault, V.; Barsella, A.; Dorkenoo, K.; Bretonnière, Y.; Andraud, C.; Mager, L.; Fontaine, L.; Odobel, F. *Chem. Mater.* **2012**, *24*, 1143. (g) Zhang, X.; Li, M.; Shi, Z.; Jin, R.; Wang, X.; Yan, Y.; Yi, M.; Zhang, D.; Cui, Z. *J. Mater. Sci.* **2011**, *46*, 4458. (h) Kim, T.-D.; Kang, J.-W.; Luo, J.; Jang, S.-H.; Ka, J.-W.; Tucker, N.; Benedict, J. B.; Dalton, L. R.; Gray, T.; Overney, R. M.; Park, D. H.; Herman, W. N.; Jen, A. K.-Y. *J. Am. Chem. Soc.* **2007**, *129*, 488. (i) Rommel, H. L.; Robinson, B. H. *J. Phys. Chem. C* **2007**, *111*, 18765. (j) DeRose, C. T.; Enami, Y.; Loychik, C.; Norwood, R. A.; Mathine, D.; Fallahi, M.; Peyghambarian, N.; Luo, J.; Jen, A. K.-Y.; Kathaperumal, M.; Yamamoto, M. *Appl. Phys. Lett.* **2006**, *89*, 131102. (k) Marder, S. R. *Chem. Commun.* **2006**, 131. (l) Locatelli, D.; Quici, S.; Roberto, D.; De Angelis, F. *Chem. Commun.* **2005**, 5405. (m) Baehr-Jones, T.; Hochberg, M.; Wang, G.; Lawson, R.; Liao, Y.; Sullivan, P. A.; Dalton, L.; Jen, A. K. Y.; Scherer, A. *Opt. Express* **2005**, *13*, 5216. (n) Dalton, L. R. *Pure Appl. Chem.* **2004**, *76*, 1421. (o) Dalton, L. *Adv. Polym. Sci.* **2002**, *158*, 1.

(3) (a) Tang, R.; Chen, H.; Zhou, S.; Xiang, W.; Tang, X.; Liu, B.; Dong, Y.; Zeng, H.; Li, Z. *Polym. Chem.* **2015**, DOI: 10.1039/C5PY00155B. (b) Virkki, M.; Tuominen, O.; Forni, A.; Saccone, M.; Metrangolo, P.; Resnati, G.; Kauranen, M.; Priimagi, A. *J. Mater. Chem. C* **2015**, *3*, 3003. (c) Zhang, Y.; Blau, W. J. *Nat. Nanotechnol.* **2015**, *10*, 205. (d) Wu, W.; Huang, L.; Song, C.; Yu, G.; Ye, C.; Liu, Y.; Qin, J.; Li, Q.; Li, Z. *Chem. Sci.* **2012**, *3*, 1256. (e) Li, Z.; Wu, W.; Li, Q.; Yu, G.; Xiao, Li.; Liu, Y.; Ye, C.; Qin, J.; Li, Z. *Angew. Chem., Int. Ed.* **2010**, *49*, 2763. (f) Gan, H.; Zhang, H.; DeRose, C. T.; Norwood, R. A.; Luo, J.; Liu, B.; Fallahi, M.; Jen, A. K.-Y.; Ho, S.-T.; Peyghambarian, N. *Proc. SPIE* **2007**, *6470*, 64700F. (g) Michalak, R. J.; Kuo, Y.-H.; Nash, F. D.; Szep, A.; Caffey, J. R.; Payson, P. M.; Haas, F.; Mckeon, B. F.; Cook, P. R.; Brost, G. A.; Luo, J.; Jen, A. K.-Y.; Dalton, L. R.; Steier, W. H. *IEEE Photonics Technol. Lett.* **2006**, *18*, 1207. (h) Dalton, L. R.; Jen, A. K.-Y.; Sullivan, P.; Eichinger, B.; Robinson, B. H. *Quantum Opt.* **2006**, *35*, 1. (i) Khan, R. U. A.; Kwon, O.-P.; Tapponnier, A.; Rashid, A. N.; Günter, P. *Adv. Funct. Mater.* **2006**, *16*, 180.

(4) (a) Sakamoto, T.; Kawanishi, T.; Tsuchiya, M. *Opt. Lett.* **2008**, *33*, 890. (b) Schmidt, W. G.; Albrecht, M.; Wippermann, S.; Blankenburg, S.; Rauls, E.; Fuchs, F.; Rodl, C.; Furthmuller, J.; Hermann, A. *Phys. Rev. B: Condens. Matter Mater. Phys.* **2008**, *77*, 035106. (c) Lucchi, F.; Janner, D.; Belmonte, M.; Balsamo, S.; Villa, M.; Giurgiola, S.; Vergani, P.; Pruneri, V. *Opt. Express* **2007**, *15*, 10739. (d) Lin, Z.; Wang, Z.; Chen, C.; Lee, M.-H. *J. Chem. Phys.* **2003**, *118*, 2349.

(5) (a) Zhou, X.-H.; Luo, J.; Davies, J. A.; Huang, S.; Jen, A. K.-Y. *J. Mater. Chem.* **2012**, *22*, 16390. (b) Piao, X.; Zhang, X.; Inoue, S.; Yokoyama, S.; Aoki, I.; Miki, H.; Otomo, A.; Tazawa, H. *Org. Electron.* **2011**, *12*, 1093. (c) Zhang, X.; Aoki, I.; Piao, X.; Inoue, S.; Tazawa, H.; Yokoyama, S.; Otomo, A. *Tetrahedron Lett.* **2010**, *51*, 5873. (d) Li, Q.; Lu, C.; Zhu, J.; Fu, E.; Zhong, C.; Li, S.; Cui, Y.; Qin, J.; Li, Z. *J. Phys. Chem. B* **2008**, *112*, 4545. (e) Gong, W.; Li, Q.; Li, Z.; Lu, C.; Zhu, J.; Li, S.; Yang, J.; Cui, Y.; Qin, J. *J. Phys. Chem. B* **2006**, *110*, 10241. (f) Liao, Y.; Bhattacharjee, S.; Firestone, K. A.; Eichinger, B. E.; Paranji, R.; Anderson, C. A.; Robinson, B. H.; Reid, P. J.; Dalton, L. R. *J. Am. Chem. Soc.* **2006**, *128*, 6847. (g) Datta, A.; Pati, S. K. *Chem. - Eur. J.* **2005**, *11*, 4961. (h) Coe, B. J.; Jones, L. A.; Harris, J. A.; Brunschwig, B. S.; Asselberghs, I.; Clays, K.; Persoons, A.; Garin, J.; Orduna, J. *J. Am. Chem. Soc.* **2004**, *126*, 3880. (i) Barlow, S.; Marder, S. R. *Chem. Commun.* **2000**, 1555. (k) Jen, A. K.-Y.; Ma, H.; Wu, X.; Wu, J.; Liu, S.; Marder, S. R.; Dalton, L. R.; Shu, C.-F. *Proc. SPIE* **1999**, *3623*, 112.

(6) (a) Isborn, C. M.; Leclercq, A.; Vila, F. D.; Dalton, L. R.; Bredas, J. L.; Eichinger, B. E.; Robinson, B. H. *J. Phys. Chem. A* **2007**, *111*, 1319. (b) Albert, I. D. L.; Marks, T. J.; Ratner, M. A. First Hyperpolaizability of Molecular Chromophores: Practical Computational Approaches. In *Progress in Organic Nonlinear Optics*; Kuzyk, M., Dirk, C. R., Eds.; Marcel Dekker: New York, 1998; pp 37−109. (c) Kanis, D. R.; Ratner, M. A.; Marks, T. J. *Chem. Rev.* **1994**, *94*, 195. (d) Marder, S. R.; Beratan, D. N.; Cheng, L.-T. *Science* **1991**, *252*, 103.

(7) (a) Alias, S.; Andreu, R.; Blesa, M. J.; Franco, S.; Garin, J.; Gragera, A.; Orduna, J.; Romero, P.; Villacampa, B.; Allain, M. *J. Org. Chem.* **2007**, *72*, 6440. (b) Andreu, R.; Blesa, M. J.; Carrasquer, L.; Garin, J.; Orduna, J.; Villacampa, B.; Alcala, R.; Casado, J.; Ruiz Delgado, M. C.; Lopez Navarrete, J. T.; Allain, M. *J. Am. Chem. Soc.* **2005**, *127*, 8835. (c) Marder, S. R.; Kippelen, B.; Jen, A. K.-Y.; Peyghambarian, N. *Nature* **1997**, *388*, 845. (d) Marder, S. R.; Cheng, L. T.; Tiemann, B. G.; Friedli, A. C.; Blanchard-Desce, M.; Perry, J. W.; Skindhoj, J. *Science* **1994**, *263*, 511.

(8) (a) Albert, I. D. L.; Marks, T. J.; Ratner, M. A. *J. Am. Chem. Soc.* **1997**, *119*, 6575. (b) Varanasi, P. R.; Jen, A. K.-Y.; Chandrasekhar, J.; Namboothiri, I. N. N.; Rathna, A. *J. Am. Chem. Soc.* **1996**, *118*, 12443.

(9) (a) Galvan-Gonzalez, A.; Belfield, K. D.; Stegeman, G. I.; Canva, M.; Marder, S. R.; Staub, K.; Levina, G.; Twieg, R. J. *J. Appl. Phys.* **2003**, *94*, 756 and references therein.

(10) (a) Dragonetti, C.; Righetto, S.; Roberto, D.; Ugo, R.; Valore, A.; Fantacci, S.; Sgamellotti, A.; De Angelis, F. *Chem. Commun.* **2007**, *40*, 4116. (b) Traber, B.; Wolff, J. J.; Rominger, F.; Oeser, T.; Gleiter, R.; Goebel, M.; Wortmann, R. *Chem. - Eur. J.* **2004**, *10*, 1227. (c) Kang, H.; Zhu, P.; Yang, Y.; Facchetti, A.; Marks, T. J. *J. Am. Chem. Soc.* **2004**, *126*, 15974. (d) Yang, M.-L.; Champagne, B. *J. Phys. Chem. A* **2003**, *107*, 3942. (e) Ostroverkhov, V.; Petschek, R. G.; Singer, K. D.; Twieg, R. J. *Chem. Phys. Lett.* **2001**, *340*, 109. (f) Quintiliani, M.; Pérez-Moreno, J.; Asselberghs, I.; Vázquez, P.; Clays, K.; Torres, T. *J. Phys. Chem. B* **2010**, *114*, 6309. (g) Akdas-Kilig, H.; Roisnel, T.; Ledoux, I.; Le Bozec, H. *New J. Chem.* **2009**, *33*, 1470. (h) Maury, O.; Le Bozec, H. *Acc. Chem. Res.* **2005**, *38*, 691.

(11) (a) Kay, A. J.; Woolhouse, A. D.; Zhao, Y.; Clays, K. *J. Mater. Chem.* **2004**, *14*, 1321. (b) Innocenzi, P.; Miorin, E.; Brusatin, G.; Abbotto, A.; Beverina, L.; Pagani, G. A.; Casalboni, M.; Sarcinelli, F.; Pizzoferrato, R. *Chem. Mater.* **2002**, *14*, 3758. (c) Kay, A. J.; Woolhouse, A. D.; Gainsford, G. J.; Haskell, T. G.; Barnes, T. H. *J. Mater. Chem.* **2001**, *11*, 996. (d) Fort, A.; Mager, L.; Muller, J.; Combellas, C.; Mathey, G.; Thiebault, A. *Opt. Mater.* **1999**, *12*, 339. (h) Andreu, R.; Carrasquer, L.; Franco, S.; Garın, J.; Orduna, J.; de Baroja, N. M.; Alicante, R.; Villacampa, B.; Allain, M. *J. Org. Chem.* **2009**, *74*, 6647. (i) Xiong, Y.; Tang, H.; Zhang, J.; Wang, Z. Y.; Campo, J.; Wenseleers, W.; Goovaerts, E. *Chem. Mater.* **2008**, *20*, 7465.

(12) (a) Sen, R.; Majumdar, D.; Bhattacharyya, S. P.; Bhattacharyya, S. N. *J. Phys. Chem.* **1993**, *97*, 7491. (b) Rettig, W. *Appl. Phys. B: Photophys. Laser Chem.* **1988**, *45*, 145. (c) Lippert, E.; Rettig, W.; Bonai-Koutecky, V.; Heisel, F.; Mieh, J. A. *Adv. Chem. Phys.* **1987**, *68*, 1.

(13) (a) Keinan, S.; Zojer, E.; Bredas, J.-L; Ratner, M. A.; Marks, T. J. *J. Mol. Struct.: THEOCHEM* **2003**, *633*, 227. (b) Albert, I. D. L.; Marks, T. J.; Ratner, M. A. *J. Am. Chem. Soc.* **1998**, *120*, 11174.

(14) (a) Shi, Y.; Lou, A. J.-T.; He, G. S.; Baev, A.; Swihart, M. T.; Prasad, P. N.; Marks, T. J. *J. Am. Chem. Soc.* **2015**, *137*, 4622. (b) Brown, E. C.; Marks, T. J.; Ratner, M. A. *J. Phys. Chem. B* **2008**, *112*, 44. (c) Wang, Y.; Frattarelli, D. L.; Facchetti, A.; Cariati, E.; Tordin, E.; Ugo, R.; Zuccaccia, C.; Macchioni, A.; Wegener, S. L.; Stern, C. L.; Ratner, M. A.; Marks, T. J. *J. Phys. Chem. C* **2008**, *112*, 8005. (d) Isborn, C. M.; Davidson, E. R.; Robinson, B. H. *J. Phys. Chem. A* **2006**, *110*, 7189. (e) Kang, H.; Facchetti, A.; Zhu, P.; Jiang, H.; Yang, Y.; Cariati, E.; Righetto, S.; Ugo, R.; Zuccaccia, C.; Macchioni, A.; Stern, C. L.; Liu, Z.; Ho, S.-T.; Marks, T. J. *Angew. Chem., Int. Ed.* **2005**, *44*, 7922.

(15) (a) Abbotto, A.; Beverina, L.; Bradamante, S.; Facchetti, A.; Klein, C.; Pagani, G. A.; Redi-Abshiro, M.; Wortmann, R. *Chem. - Eur. J.* **2003**, *9*, 1991. (b) Bradamante, S.; Facchetti, A.; Pagani, G. A. *J. Phys. Org. Chem.* **1997**, *10*, 514. (c) Albert, I. D. L.; Marks, T. J.; Ratner, M. A. *J. Am. Chem. Soc.* **1997**, *119*, 6575. (d) Wong, K. Y.; Jen, A. K.-Y.; Rao, V. P. *Phys. Rev. A: At., Mol., Opt. Phys.* **1994**, *49*, 3077. (e) Dirk, C. W.; Katz, H. E.; Schilling, M. L.; King, A. L. *Chem. Mater.* **1990**, *2*, 700. (f) Katritzky, R. *Handbook of Heterocyclic Chemistry*; Pergamon Press: Oxford, 1983.

(16) (a) Cheng, Y.-J.; Luo, J.; Huang, S.; Zhou, X.; Shi, Z.; Kim, T.-D.; Bale, D. H.; Takahashi, S.; Yick, A.; Polishak, B. M.; Jang, S.-H.; Dalton, L. R.; Reid, P. J.; Steier, W. H.; Jen, A. K.-Y. *Chem. Mater.* **2008**, *20*, 5047. (b) Toutchkine, A.; Nguyen, D.-V.; Hahn, K. M. *Org. Lett.* **2007**, *9*, 2775. (c) Yogo, T.; Urano, Y.; Ishitsuka, Y.; Maniwa, F.; Nagano, T. *J. Am. Chem. Soc.* **2005**, *127*, 12162. (d) Renikuntla, B. R.; Rose, H. C.; Eldo, J.; Waggoner, A. S.; Armitage, B. A. *Org. Lett.* **2004**, *6*, 909. (e) Bug, T.; Mayr, H. *J. Am. Chem. Soc.* **2003**, *125*, 12980. (f) Weir, C. A. M.; Hadizad, T.; Beaudin, A. M. R.; Wang, Z. Y. *Tetrahedron Lett.* **2003**, *44*, 4697. (g) Ren, Y.; Szablewski, M.; Cross, G. H. *Appl. Opt.* **2000**, *39*, 2499. (h) Dam, N.; Scurlock, R. D.; Wang, B.; Ma, L.; Sundahl, M.; Ogilby, P. R. *Chem. Mater.* **1999**, *11*, 1302. (i) Lux, A.; Holmes, A. B.; Cervini, R.; Davies, J. E.; Moratti, S. C.; Gruner, J.; Cacialli, F.; Friend, R. H. *Synth. Met.* **1997**, *84*, 293.

(j) Prein, M.; Adam, W. *Angew. Chem., Int. Ed. Engl.* **1996**, *35*, 477. (k) Scurlock, R. D.; Wang, B.; Ogilby, P. R.; Sheats, J. R.; Clough, R. L. *J. Am. Chem. Soc.* **1995**, *117*, 10194. (l) Hama, Y.; Nobuhara, Y.; Aso, Y.; Otsubo, T. *Bull. Chem. Soc. Jpn.* **1988**, *61*, 1683. (m) Suchanski, M. R.; Van Duyne, R. P. *J. Am. Chem. Soc.* **1976**, *98*, 250.

(17) (a) Klan, P. *Monatsh. Chem.* **1993**, *124*, 327. (b) Diemer, V.; Chaumeil, H.; Defoin, A.; Fort, A.; Boeglin, A.; Carré, C. *Eur. J. Org. Chem.* **2008**, *2008*, 1767.

(18) Helms, A.; Heiler, D.; McLendon, G. *J. Am. Chem. Soc.* **1992**, *114*, 6227.

(19) (a) Yin, J.; Rainka, M. P.; Zhang, X.-X.; Buchwald, S. L. *J. Am. Chem. Soc.* **2002**, *124*, 1162. (b) Barder, T. E.; Walker, S. D.; Martinelli, J. R.; Buchwald, S. L. *J. Am. Chem. Soc.* **2005**, *127*, 4685. (c) Walker, S. D.; Barder, T. E.; Martinelli, J. R.; Buchwald, S. L. *Angew. Chem.* **2004**, *116*, 1907. (d) Martin, R.; Buchwald, S. L. *Acc. Chem. Res.* **2008**, *41*, 1461.

(20) Tanner, J. *J. Chem. Phys.* **1970**, *52*, 2523.

(21) Mills, R. *J. Phys. Chem.* **1973**, *77*, 685. Data at different temperatures were estimated by interpolation of the data reported by Mills, giving $D_{HDO} = 1.780 \times 10^{-9}$ m^2 s^{-1} at 295.7 K.

(22) (a) The viscosity of CD$_2$Cl$_2$ was estimated to be 0.4256 cP at 295.7 K by interpolation of the data reported for CH$_2$Cl$_2$: *CRC Handbook of Chemistry and Physics*, 67th ed.; Weast, R. C., Ed.; Chemical Rubber Co.: Cleveland, OH, 1986 (b) The viscosity of DMSO-d_6 was estimated to be 2.138 cP at 295.7 K by interpolation of the data reported for DMSO: Higashigaki, Y.; Christensen, D. H.; Wang, C. H. *J. Phys. Chem.* **1981**, *85*, 2531. (c) Both values are corrected for the reduced mass as proposed by Holz et al.: Holz, M.; Mao, X.; Seiferling, D.; Sacco, A. *J. Chem. Phys.* **1996**, *104*, 669.

(23) Zuccaccia, D.; Macchioni, A. *Organometallics* **2005**, *24*, 3476.

(24) (a) Levine, B. F.; Bethea, C. G. *Appl. Phys. Lett.* **1974**, *24*, 445. (b) Singer, K. D.; Garito, A. F. *J. Chem. Phys.* **1981**, *75*, 3572. (c) Ledoux, I.; Zyss. *Chem. Phys.* **1982**, *73*, 203.

(25) (a) Kanis, D. R.; Lacroix, P. G.; Ratner, M. A.; Marks, T. J. *J. Am. Chem. Soc.* **1994**, *116*, 10089. (b) Roberto, D.; Ugo, R.; Bruni, S.; Cariati, E.; Cariati, F.; Fantucci, P.; Invernizzi, I.; Quici, S.; Ledoux, I.; Zyss, J. *Organometallics* **2000**, *19*, 1775. (c) Lesley, M. J. G.; Woodward, A.; Taylor, N. J.; Marder, T. B.; Cazenobe, I.; Ledoux, I.; Zyss, J.; Thornton, A.; Bruce, D. W.; Kakkar, A. K. *Chem. Mater.* **1998**, *10*, 1355.

(26) *Jaguar 4.2*; Schrödinger, Inc.: Portland, OR, 1991−2000.

(27) (a) Becke, A. D. *Phys. Rev. A: At., Mol., Opt. Phys.* **1988**, *38*, 3098. (b) Lee, C.; Yang, W.; Parr, R. G. *Phys. Rev. B: Condens. Matter Mater. Phys.* **1988**, *37*, 785.

(28) Feller, D.; Davidson, E. R. Basis Sets for Ab Initio Molecular Orbital Calculations and Intermolecular Interactions. In *Reviews in Computational Chemistry*; Lipkowitz, K. B., Boyd, D. B., Eds.; VCH Publishers, Inc.: New York, 1990; Vol. *1*, p 1.

(29) Ridley, J.; Zerner, M. *Theor. Chim. Acta* **1973**, *32*, 111.

(30) Zeng, J.; Hush, N. S.; Reimers, J. R. *J. Am. Chem. Soc.* **1996**, *118*, 2059.

(31) Meyers, F.; Marder, S. R.; Pierce, B. M.; Bredas, J.-L. *J. Am. Chem. Soc.* **1994**, *116*, 10703.

(32) Orr, B. J.; Ward, J. F. *Mol. Phys.* **1971**, *20*, 513.

(33) Balicki, R.; Kaczmarek, L. *Gazz. Chim. Ital.* **1994**, *124*, 385.

(34) Wolfe, J. P.; Ahman, J.; Sadighi, J. P.; Singer, R. A.; Buchwald, S. L. *Tetrahedron Lett.* **1997**, *38*, 6367.

(35) Abbotto, A.; Bradamante, S.; Facchetti, A.; Pagani, G. A. *J. Org. Chem.* **1997**, *62*, 5755.

(36) For an approach to stabilizing carbanion donors, see: Beverina, L.; Sanguineti, A.; Battagliarin, G.; Ruffo, R.; Roberto, D.; Righetto, S.; Soave, R.; Lo Presti, L.; Ugo, R.; Pagani, G. A. *Chem. Commun.* **2011**, *47*, 292.

(37) Database of average bond lengths in organic compounds: Allen, F. H.; Kennard, O.; Watson, D. G.; Brammer, L.; Orpen, A. G.; Taylor, R. *J. Chem. Soc., Perkin Trans. 2* **1987**, S1.

(38) Fröhlich, R.; Musso, H. *Chem. Ber.* **1985**, *118*, 4649.

(39) Bhaskaran, S.; Velmurugan, D.; Ravikumar, K.; Mohanakrishnan, A. K.; Prakash, C. *Anal. Sci.: X-Ray Struct. Anal. Online* **2005**, *21*, 199.

(40) Cole, J. C.; Cole, J. M.; Cross, G. H.; Farsari, M. J.; Howard, A. K.; Szablewski, M. *Acta Crystallogr., Sect. B: Struct. Sci.* **1997**, *53*, 812.

(41) Das, A.; Jeffery, J. C.; Maher, J. P.; McCleverty, J. A.; Schatz, E.; Ward, M. D.; Wollermann, G. *Inorg. Chem.* **1993**, *32*, 2145.

(42) Alfalah, S.; Deeb, O.; Zilberg, S.; Haas, Y. *Chem. Phys. Lett.* **2008**, *459*, 100.

(43) Würthner, F.; Yao, S.; Debaerdemaeker, T.; Wortmann, R. *J. Am. Chem. Soc.* **2002**, *124*, 9431.

(44) Pandey, S.; Kar, J. R.; Azam, A.; Pandey, S.; Chawla, H. M. *J. Solution Chem.* **2010**, *39*, 107.

(45) Reichardt, C. *Chem. Rev.* **1994**, *94*, 2319.

(46) Citterio, D.; Kawada, T.; Yagi, J.; Ishigaki, T.; Hisamoto, H.; Sasaki; Suzuki, K. *Anal. Chim. Acta* **2003**, *482*, 19.

(47) *Solvents and Solvent Effects in Organic Chemistry 2*; Reichardt, C., Ed.; VCH: Weinheim, 1990.

(48) Chen, C.-T.; Marder, S. R. *Adv. Mater.* **1995**, *7*, 1030.

(49) Szablewski, M.; Thomas, P. R.; Thornton, A.; Bloor, D.; Cross, G. H.; Cole, J. M.; Howard, J. A. K.; Malagoli, M.; Meyers, F.; Brédas, J.-L.; Wenseleers, W.; Goovaerts, E. *J. Am. Chem. Soc.* **1997**, *119*, 3144.

(50) Thelakkat, M.; Schmidt, H.-W. *Adv. Mater.* **1998**, *10*, 219.

(51) (a) Würthner, F.; Wortmann, R.; Meerholz, K. *ChemPhysChem* **2002**, *3*, 17. (b) Halter, M.; Liao, Y.; Plocinik, R. M.; Coffey, D. C.; Bhattacharjee, S.; Mazur, U.; Simpson, G. J.; Robinson, B. H.; Keller, S. L. *Chem. Mater.* **2008**, *20*, 1778. (c) Song, Q.; Evans, C. E.; Bohn, P. W. *J. Phys. Chem.* **1993**, *97*, 13736. (d) Nakahara, H.; Möbius, D. *J. Colloid Interface Sci.* **1986**, *114*, 363. (e) Levitus, M.; Schmieder, K.; Ricks, H.; Shimizu, K. D.; Bunz, U. H. F.; Garcia-Garibay, M. A. *J. Am. Chem. Soc.* **2001**, *123*, 4259. (f) Datta, A.; Pati, S. K. *Chem. Soc. Rev.* **2006**, *35*, 1305. (g) Pizzotti, M.; Tessore, F.; Biroli, A. O.; Ugo, R.; De Angelis, F.; Fantacci, S.; Sgamellotti, A.; Zuccaccia, D.; Macchioni, A. *J. Phys. Chem. C* **2009**, *113*, 11131.

(52) (a) Avram, L.; Cohen, Y. *Chem. Soc. Rev.* **2015**, *44*, 586. (b) Macchioni, A.; Ciancaleoni, G.; Zuccaccia, C.; Zuccaccia, D. Diffusion Ordered NMR Spectroscopy (DOSY). In *Supramolecular Chemistry: From Molecules to Nanomaterial*; Gale, P. A., Steed, J. W., Eds.; John Wiley & Sons, Ltd.: New York, 2012; Vol. 2, Ch. 4 (ISBN: 978-0-470-74640-0).

(53) Macchioni, A.; Ciancaleoni, G.; Zuccaccia, C.; Zuccaccia, D. *Chem. Soc. Rev.* **2008**, *37*, 479.

(54) (a) Theoretical expressions of *f* have been obtained for prolate or oblate ellipsoids by Perrin: Perrin, F. *J. Phys. Radium* **1936**, *7*, 1. (b) The corresponding expression for ellipsoids having three unequal axes was obtained by Elworthy: Elworthy, P. H. *J. Chem. Soc.* **1962**, 3718.

(55) (a) Wong, M. S.; Bosshard, C.; Günter, P. *Adv. Mater.* **1997**, *9*, 837. (b) Li, Q.; Li, Z.; Ye, C.; Qin, J. *J. Phys. Chem. B* **2008**, *112*, 4928. (c) Li, Z.; Li, Z.; Di, C.; Zhu, Z.; Li, Q.; Zeng, Q.; Zhang, K.; Liu, Y.; Ye, C.; Qin, J. *Macromolecules* **2006**, *39*, 6951. (d) Luo, J.; Zhou, X.-H.; Jen, A. K.-Y. *J. Mater. Chem.* **2009**, *19*, 7410. (e) Liakatas, I.; Cai, C.; Bosch, M.; Jager, M. *Appl. Phys. Lett.* **2000**, *76*, 1368. (f) Xiong, Y.; Tang, H.; Zhang, J.; Wang, Z. Y. *Chem. Mater.* **2008**, *20*, 7465.